Calhoun: The NPS Institutional Archive

DSpace Repository

Theses and Dissertations | 1. Thesis and Dissertation Collection, all items

1987

Microstructural characterization of HSLA-100 GMA-weldme

Mickelberry, Kenneth D.; Challenger, Kenneth D.

http://hdl.handle.net/10945/22362

Downloaded from NPS Archive: Calhoun

http://www.nps.edu/library

Calhoun is the Naval Postgraduate School's public access digital repository for research materials and institutional publications created by the NPS community. Calhoun is named for Professor of Mathematics Guy K. Calhoun, NPS's first appointed -- and published -- scholarly author.

Dudley Knox Library / Naval Postgraduate School
411 Dyer Road / 1 University Circle
Monterey, California USA 93943

NAVAL POSTGRADUATE SCHOOL
MONTEREY, CALIFORNIA 93943-5002

NAVAL POSTGRADUATE SCHOOL
Monterey, California

THESIS

MICROSTRUCTURAL CHARACTERIZATION
OF HSLA-100 GMA-WELDMENTS

by

Kenneth Dalton Mickelberry

September 1987

Thesis Advisor: K.D. Challenger

Approved for public release; distribution unlimited.

T234292

SECURITY CLASSIFICATION OF THIS PAGE

REPORT DOCUMENTATION PAGE

1a REPORT SECURITY CLASSIFICATION: UNCLASSIFIED	1b RESTRICTIVE MARKINGS
2a SECURITY CLASSIFICATION AUTHORITY	3 DISTRIBUTION/AVAILABILITY OF REPORT: Approved for public release; distribution unlimited.
2b DECLASSIFICATION/DOWNGRADING SCHEDULE	
4 PERFORMING ORGANIZATION REPORT NUMBER(S)	5 MONITORING ORGANIZATION REPORT NUMBER(S)
6a NAME OF PERFORMING ORGANIZATION: Naval Postgraduate School; 6b OFFICE SYMBOL (If applicable): 69	7a NAME OF MONITORING ORGANIZATION: Naval Postgraduate School
6c ADDRESS (City, State, and ZIP Code): Monterey, California 93943-5000	7b ADDRESS (City, State, and ZIP Code): Monterey, California 93943-5000
8a NAME OF FUNDING/SPONSORING ORGANIZATION; 8b OFFICE SYMBOL (If applicable)	9 PROCUREMENT INSTRUMENT IDENTIFICATION NUMBER
8c ADDRESS (City, State, and ZIP Code)	10 SOURCE OF FUNDING NUMBERS: PROGRAM ELEMENT NO; PROJECT NO; TASK NO; WORK UNIT ACCESSION NO

11 TITLE (Include Security Classification)

MICROSTRUCTURAL CHARACTERIZATION OF HSLA-100 GMA-WELDMENTS

12 PERSONAL AUTHOR(S): Mickelberry Kenneth D.

13a TYPE OF REPORT	13b TIME COVERED	14 DATE OF REPORT (Year Month Day)	15 PAGE COUNT
Master's Thesis:	FROM _____ TO _____	September 1987	69

16 SUPPLEMENTARY NOTATION

17 COSATI CODES			18 SUBJECT TERMS (Continue on reverse if necessary and identify by block number)
FIELD	GROUP	SUB-GROUP	HSLA-100 GMA-Weldments

19 ABSTRACT (Continue on reverse if necessary and identify by block number)

A high strength low alloy steel, HSLA-100, is under development by the U.S. Navy. Instead of developing a new weld filler metal for this alloy it is desirable to use the already certified filler metals that are used for welding HY-100 steel. The research presented in this thesis evaluated the effect of cooling rate on the HY-100 welding consumable when used to weld HSLA-100 plate. The 800 ^{o}C to 500 ^{o}C cooling rate after gas metal arc welding was varied from 22 ^{o}C/sec to 42 ^{o}C/sec by using different plate thickness, different preheat and interpass temperatures as well as different heat inputs. Mechanical property data is reported elsewhere but summarized in this thesis.

20 DISTRIBUTION/AVAILABILITY OF ABSTRACT	21 ABSTRACT SECURITY CLASSIFICATION
☒ UNCLASSIFIED/UNLIMITED ☐ SAME AS RPT ☐ DTIC USERS	UNCLASSIFIED
22a NAME OF RESPONSIBLE INDIVIDUAL: Kenneth D. Challenger	22b TELEPHONE (Include Area Code): 408-646-2081; 22c OFFICE SYMBOL: 69Ch

DD FORM 1473, 84 MAR — 83 APR edition may be used until exhausted. All other editions are obsolete.

SECURITY CLASSIFICATION OF THIS PAGE

UNCLASSIFIED

#19 - ABSTRACT - CONTINUED

All welds met required strength and toughness. However, for all but the fastest cooling rate, the tensile test transverse to the weld failed in the weld metal rather than in the base metal as would be expected with HY-100 steel. This indicates that the weld metal strength is less that the base metal, an undesirable situation.

The weld metal microstructure was characterized by optical metallography, scanning and transmission electron microscopy. These microstructures were correlated with microhardness and the mechanical properties. All welds have a predominately acicular ferrite microstructure. Occasional regions of side plate ferrite and MAC (martensite, austenite and carbide combinations) were observed but not believed to have any significant effect on the mechanical behavior. Retained austenite was often observed between the ferrite laths when examined by transmission electron microscopy. This austenite is believed to be very stable and may be responsible for the excellent resistance to brittle fracture exhibited by these welds.

Approved for public release; distribution unlimited.

Microstructural Characterization of HSLA-100 GMA-Weldments

by

Kenneth D. Mickelberry
Lieutenant, United States Navy
B.S., University of Houston, 1978

Submitted in partial fulfillment of the
requirements for the degree of

MASTER OF SCIENCE IN MECHANICAL ENGINEERING

from the

NAVAL POSTGRADUATE SCHOOL
September 1987

NPS-55
C.1

ABSTRACT

A high strength low alloy steel, HSLA-100, is under development by the U.S. Navy. Instead of developing a new weld filler metal for this alloy it is desirable to use the already certified filler metals that are used for welding HY-100 steel. The research presented in this thesis evaluated the effect of cooling rate on the HY-100 welding consumable when used to weld HSLA-100 plate. The 800 ^{o}C to 500 ^{o}C cooling rate after gas metal arc welding was varied from 22 ^{o}C/sec to 42 ^{o}C/sec by using different plate thickness, different preheat and interpass temperatures as well as different heat inputs. Mechanical property data is reported elsewhere but summarized in this thesis.

All welds met required strength and toughness. However, for all but the fastest cooling rate, the tensile test transverse to the weld failed in the weld metal rather than in the base metal as would be expected with HY-100 steel. This indicates that the weld metal strength is less that the base metal, an undesirable situation.

The weld metal microstructure was characterized by optical metallography, scanning and transmission electron microscopy. These microstructures were correlated with microhardness and the mechanical properties. All welds have a predominately acicular ferrite microstructure. Occasional regions of side plate ferrite and MAC (martensite, austenite and carbide combinations) were observed but not believed to have any significant effect on the mechanical behavior.

Retained austenite was often observed between the ferrite laths when examined by transmission electron microscopy. This austenite is believed to be very stable and may be responsible for the excellent resistance to brittle fracture exhibited by these welds.

TABLE OF CONTENTS

I. INTRODUCTION - 11
II. BACKGROUND - 12
III. EXPERIMENTAL PROCEDURE - - - - - - - - - - - - - - 15
A. MATERIAL - 15
B. MACROSAMPLE PREPARATION - - - - - - - - - - - - 15
C. MICROHARDNESS TESTING - - - - - - - - - - - - - 16
D. OPTICAL MICROSCOPY - - - - - - - - - - - - - - 16
E. SCANNING ELECTRON MICROSCOPY - - - - - - - - - 17
F. TRANSMISSION ELECTRON MICROSCOPY - - - - - - - 17
G. TENSILE AND IMPACT TESTING - - - - - - - - - - 18
IV. RESULTS - 19
A. TENSILE AND IMPACT PROPERTIES - - - - - - - - - 19
B. MICROHARDNESS TRAVERSES - - - - - - - - - - - - 20
C. METALLOGRAPHY - - - -- - - - - - - - - - - - - 21
V. DISCUSSION OF RESULTS - - - - - - - - - - - - - - 25
VI. CONCLUSIONS - - - - - - - - - - - - - - - - - - - 28
VII. RECOMMENDATIONS- - - - - - - - - - - - - - - - - - 29
APPENDIX: TABLES AND FIGURES- - - - - - - - - - - - - - 30
LIST OF REFERENCES - - - - - - - - - - - - - - - - - - 67
INITIAL DISTRIBUTION LIST - - - - - - - - - - - - - - 68

LIST OF TABLES

1. Chemical Composition of Base Plate, Filler Wire and Weld Metal - - - - - - - - - - - 30
2. Tensile Properties of the Base Metal - - - - - 31
3. Welding Conditions for HSLA-100 Weldments- - - - 32
4. Tensile Properties of the Weld Metal - - - - - - 33
5. Impact Properties of the Weld Metal - - - - - - 34
6. Cooling Rate vs. Microhardness Mean and Standard Deviation - - - - - - - - - - - - 35
7. Cooling Rate vs. Average Lath Width - - - - - - 36

LIST OF FIGURES

1. Optical Micrograph of W130 Base Metal - - - - - - 37
2. Optical Micrograph of W123 Base Metal - - - - - - 37
3. 19 mm Thick Plate as Received - - - - - - - - - - 38
4. 19 mm Thick Plate as Received - - - - - - - - - - 38
5. 6.35 mm Thick Plate as Received - - - - - - - - - 39
6. 6.35 mm Thick Plate as Received - - - - - - - - - 39
7. Macrosample of W130 - - - - - - - - - - - - - - - 40
8. Macrosample of W119 - - - - - - - - - - - - - - - 41
9. Macrosample of W125 - - - - - - - - - - - - - - - 42
10. Macrosample of W123 - - - - - - - - - - - - - - - 42
11. Three Dimensional Topography of W130 - - - - - - 43
12. Sketch of Mounted W130 Sample - - - - - - - - - - 43
13. Three Dimensional Topography of W119 - - - - - - 44
14. Sketch of Mounted W119 Sample - - - - - - - - - - 44
15. Three Dimensional Topography of W125 - - - - - - -45
16. Sketch of Mounted W125 Sample - - - - - - - - - - 45
17. Three Dimensional Topography of W123 - - - - - - -46
18. Sketch of Mounted W123 Sample - - - - - - - - - - 46
19. DBTT Curve -47
20. Vickers Hardness Traverse of W130 - - - - - - - - 48
21. Vickers Hardness Traverse of W119 - - - - - - - - 49
22. Vickers Hardness Traverse of W125 - - - - - - - - 50
23. Vickers Hardness Traverse of W123 - - - - - - - - 51
24. Solidification Structure W130 - - - - - - - - - - 52
25. Solidification Structure W119 - - - - - - - - - - 53
26. Solidification Structure W125 - - - - - - - - - - 54
27. Solidification Structure W123 - - - - - - - - - - 55
28. Micrographs of W130 (41.7°C/sec) - - - - - - - - 56
    A.) 334 HV Optical Micrograph - - - - - - - - - - 56
    B.) 297 HV Optical Micrograph - - - - - - - - - - 56
    C.) 258 HV Optical Micrograph - - - - - - - - - - 56
    D.) 334 HV SEM Micrograph - - - - - - - - - - - - 56
    E.) 297 HV SEM Micrograph - - - - - - - - - - - - 56
    F.) 258 HV SEM Micrograph - - - - - - - - - - - - 56

29. Micrographs of W119 (20.4°C/sec)- - - - - - - - - 57
A.) 301 HV Optical Micrograph - - - - - - - - - - 57
B.) 271 HV Optical Micrograph - - - - - - - - - - 57
C.) 265 HV Optical Micrograph - - - - - - - - - - 57
D.) 301 HV SEM Micrograph - - - - - - - - - - - 57
E.) 271 HV SEM Micrograph - - - - - - - - - - - 57
F.) 265 HV SEM Micrograph - - - - - - - - - - - 57

30. Micrographs of W125 (33.4°C/sec) - - - - - - - - 58
A.) 327 HV Optical Micrograph - - - - - - - - - - 58
B.) 305 HV Optical Micrograph - - - - - - - - - - 58
C.) 297 HV Optical Micrograph - - - - - - - - - - 58
D.) 327 HV SEM Micrograph - - - - - - - - - - - 58
E.) 305 HV SEM Micrograph - - - - - - - - - - - 58
F.) 297 HV SEM Micrograph - - - - - - - - - - - 58

31. Micrographs of W123 (21.6°C/sec) - - - - - - - - 59
A.) 330 HV Optical Micrograph - - - - - - - - - - 59
B.) 293 HV Optical Micrograph - - - - - - - - - - 59
C.) 216 HV Optical Micrograph - - - - - - - - - - 59
D.) 330 HV SEM Micrograph - - - - - - - - - - - 59
E.) 293 HV SEM Micrograph - - - - - - - - - - - 59
F.) 216 HV SEM Micrograph - - - - - - - - - - - 59

32. TEM Micrograph of W130
A.) Inclusions, Acicular Ferrite and Laths in the Weld Metal- - - - - - - - - - - 60
B.) Inclusions and Laths in the Fusion Line Thin Foil Sample - - - - - - - - - - - 60

33. TEM Micrograph of W125
A.) Inclusions, Laths and Retained Austenite in the Weld Metal - - - - - - - - - 61
B.) Inclusions, Laths in Weld Metal - - - - - - 61

34. TEM Micrograph of
A.) Dislocations and Laths in W119 Weld Metal Sample - - - - - - - - - - - - - - 62
B.) Inclusions and Large Grains on the W123 Fusion Line - - - - - - - - - - - 62

35. Tem Micrograph of W119
A.) Dislocations and Laths in the Weld Metal - - - - - - - - - - - - - - - 63
B.) Dislocations and Precipitates - - - - - - - 63

36. TEM Micrograph of W125
A.) Weld Metal - - - - - - - - - - - - - - - - - - 64
B.) Micro Twins - - - - - - - - - - - - - - - - - 64

37. TEM Micrograph of
A.) W123 Weld Metal Retained Austenite - - - - - 65
B.) W119 Fusion Line TEM - - - - - - - - - - - - 65

38. CCT Curve for Oxygen Inclusions
A.) Low Oxygen Regime - - - - - - - - - - - - - - 66
B.) High Oxygen Regime - - - - - - - - - - - - - 66
C.) Intermediate Oxygen Regime - - - - - - - - 66
D.) Schematic CCT Diagram - - - - - - - - - - - 66

ACKNOWLEDGEMENTS

I wish to express my appreciation to my thesis advisor, Professor K.D. Challenger. I also want to thank Dr. J.M.B. Loez for his superb transmission electron microscopy work as well as his guidance, help and much appreciated encouragement.

Additionally I want to thank my parents who have been very patient while spending much of their vacation waiting for their son to finish his thesis. But even more I want to thank them for all their love and support over the years.

I. INTRODUCTION

High strength low alloy (HSLA) steels are receiving increased attention as the search for a high strength steel which will be economical, as well as practical, to weld continues. By using a low carbon, precipitation-hardened steel many of the problems associated with high carbon steels can be avoided and the cost of welding can be reduced as discussed in NAVSEA's Material Fabrication Improvement goals for fiscal years 1983 through 1990. With the prime goal of this program being to "reduce shipbuilding costs through improvement of welding processes, materials, technologies, procedures, and techniques, while simultaneously improving overall quality"; a copper precipitation strengthened HSLA steel with nickel added for toughness and strength appears to be one of the most promising methods of meeting these goals (Ref. 1).

However, before certification for ship construction, the various common welding processes and their required filler metals must be qualified. This is done by extensive mechanical testing as well as microstructural evaluation.

This research investigates the effect of weld metal cooling rates on the microstructure, microhardness, yield strength and impact properties of GMAW weldments. Attempts to identify the major microstructural constituents and correlate them with mechanical property data presently available in the literature was also performed.

II. BACKGROUND

The Navy has qualified a low carbon, copper precipitation strengthened steel, HSLA-80 (MIL-S-24645) for ship construction. HSLA-80 (550 MPa yield strength) has been shown to exhibit excellent weldability and fracture toughness when welded without preheat in plate thicknesses up to 19mm (3/4 in) (Ref 2). It was with this knowledge and experience that the baseline composition of the HSLA-100 (690 MPa yield strength) was specified (Ref. 3). HSLA-100 steel is being evaluated to determine if it is also suitable for general use in construction of ships and submarines.

Funded by the SSN-21 Design Support Program under the technical monitoring of David Taylor Naval Ship Research and Development Center (DTNSRDC), AMAX Materials Research Center (AMRC) was contracted to develop an HSLA steel composition to meet the strength and toughness of HY-100 (High Yield) steel. Under Phase II of contract N00167-85-C-0066 two thicknesses (6.35mm [1/4 inch] and 19 mm [3/4 inch]) of HSLA-100 plates were produced. Table 1 lists the chemical composition of the 6.35 mm base plate which is representative of both plates. The 6.35 mm plate was austenititized at 900^{o}C (1650^{o}F) for 15 minutes, water quenched, aged at 690^{o}C (1275^{o}F) for 45 minutes and air cooled. The 19 mm plate was austenitized at 900^{o}C for 45 minutes water quenched, aged at 635^{o}C (1175^{o}F) for 60 minutes and air cooled. Figures 1 and 2 show the base plate microstructure which is composed primarily of upper bainite. The mechanical properties of the base material

are listed in Table 2. It can be seen from this table that both plate thicknesses exceed the required 690 MPa (100 ksi) yield strength.

HSLA steels employ the use of several strengthening mechanisms, including grain refinement, precipitation strengthening, solid solution strengthening and transformation-induced substructure strengthening. The increase in strengthening from 80 ksi to 100 ksi must come from transformation substructure and precipitation strengthening since the contribution to yield strength from solid-solution effects is relatively small and the degree of grain refinement from the presence of 0.02 to 0.06% niobium would be essentially the same as the HSLA-80 steel. The same hardenability elements of Mn, Ni, Cr, and Mo present in HSLA-80 were also included in the HSLA-100 composition with Ni protecting against hot shortness as well as increasing toughness (Ref. 3).

Studies on the effects of various heat treatments on the mechanical properties and microstructure of HSLA steels similar to HSLA-80 have been performed. Since properties after welding are controlled to a large extent by the thermal cycle of the weld process these heat treatment studies may be germane. One study (Ref. 4) examined the grain structure, inclusion content, and precipitate types present after six different heat treatments. They concluded that a higher austenitizing temperature combined with water-quenching resulted in an acicular ferrite microstructure, while lower temperatures produced equiaxed ferrite or ferrite-pearlite structures. It has been know for some time that an acicular ferrite is the most desirable microstructure in weld metal. Additionally, it has been shown that toughness in HSLA weldments is controlled by weld metal microstructure (Ref. 5).

The welds in this study (provided by DTNSRDC) are multipass weldments. Multipass welding provides microstructural refinement in the weld metal which normally improves toughness and reduces residual stresses (Ref. 6). Three of the four weld samples were welded using the temper bead sequence while W123 was not.

Table 1 also lists for comparison the chemical compositions of the filler wire and the weld metal. The 120-s wire has been used extensively as an HY-100 filler metal but has not been studied in depth since most of the problems associated with HY-100 weldments were in the heat affected zone (HAZ). The chemical composition of the weld metal differs from the wire composition because of mixing between the melted base plate and the filler metal.

III. EXPERIMENTAL PROCEDURE

A. MATERIAL

The GMAW-S (Gas Metal Arc Weld - Spray transfer) weldments were found by DTNSRDC to have satisfactory tensile and impact properties, therefore were selected for further study. Two of the weldments were from 19mm (3/4 inch) thick plates (Figures 3 and 4) and two were from 6.35mm (1/4 in) thick plates (Figures 5 and 6). Table 3 lists the welding conditions required to obtain the cooling rates desired for investigation. This table includes the weld numbers, plate thickness, preheat/interpass temperatures, heat input and average cooling rate between 800°C and 500°C. Various combinations of plate thickness, preheat temperature and heat input were used to generate these cooling rates. Joint design was a sixty degree double-V groove with a backing plate for three of the samples while W119 was a single V joint.

B. MACROSAMPLE PREPARATION

Upon receipt from DTNSRDC the plates were cut lengthwise (perpendicular to the welding direction) into approximately 25 mm (1 inch) thick sections along a scribed line as shown by the arrows in Figures 3 and 5. The base material ends were cut off under flooded lubrication in order not to change any microstructural characteristics of the material. The arrows in Figures 4 and 6 indicate where these cuts were made and that a safe margin was added in order to include all of the heat affected zone. The region containing the weld metal and the heat affected zone (HAZ) was then cold

sanded and polished in order to produce a smooth flat surface suitable for macroetching. Various solutions were tried including 2% nital, Oberhoffer's etch, and ammonium persulfate. The etch which produced the best results was 2% nital in which the samples were submerged for about 10 minutes exposing the desired characteristics. Figures 7 to 10 illustrate the prepared macrosamples of each weldment.

C. MICROHARDNESS TESTING

Each sample was cut under flooded lubrication to separate the weld metal from the HAZ and the base metal as shown in Figures 11, 13, 15, and 17. The weld metal samples were metallographically mounted, and polished using diamond paste of 1 micron and 0.5 microns. They were then etched with 2 vol% nital before microhardness traverses were performed on each specimen. A scribe and a straight edge were used to mark a line across the sample as shown in Figures 12, 14, 16, and 18, in order to more easily locate the hardness traverse during photography. The hardness traverse was taken parallel to the line approximately 1.0 mm away from it with penetrations made at 0.25 mm intervals. Vickers microhardness measurements were made using a diamond indenter and a 300 g load.

D. OPTICAL MICROSCOPY

Upon completion of the microhardness traverses the weld samples were examined under a Zeiss Universal Research Photomicroscope. A series of micrographs were taken along the microhardness traverse with the microhardness indentations serving as references points. Each area was carefully viewed in order to characterize the microstructure and correlate it with

the Vickers hardness readings. Additionally, the samples were etched in Oberhoffer's etch and photographed at 50x to show the solidification structure of the weld metal. A montage of this structure was produced for each specimen.

E. SCANNING ELECTRON MICROSCOPY

The specimens were left in their mounts and examined under the Cambridge Stereo Scan S4-10 Scanning Electron Microscope (SEM). The same areas that were of interest in light microscopy were examined. Again using the microhardness indentations as reference points, 2000X micrographs of the highest, intermediate and lowest hardness areas were taken.

F. TRANSMISSION ELECTRON MICROSCOPY

Figures 11, 13, 15 and 17 depict the exact locations examined using a JOEL JEM-120CX MK II Transmission Electron Microscope (TEM). One area was in the weld metal and the other was on the fusion line. The weld metal TEM specimens were cut transversely from the weld metal samples using an ISOMET low speed wafering machine. Several slices 0.20 mm were cut and then each slice was hand sanded down to 0.15 mm. From the 0.15 mm sample 3 mm diameter discs were punched out for further thinning in a Struers Tenupol apparatus. The electrolyte, consisted of 10% percloric acid and 90% acetic acid at a temperature of 13^{o}C (55^{o}F). The power supply was set at 50-60 volts resulting in a current of 180 - 200 milliamps. The medium flowrate setting on the Tenupol was used in conjunction with the sensitivity of the photo cell circuit adjusted to terminate electropolishing upon initial penetration. The thin foils were then examined in the TEM.

G. TENSILE AND IMPACT TESTING

All the tensile and impact testing was performed by David Taylor Naval Ship Research and Development Center. As mentioned, Table 4 lists the tensile test properties for the weld metal while Table 5 lists the impact test properties.

IV. RESULTS

A. TENSILE AND IMPACT PROPERTIES

Table 4 lists the tensile properties of the weld metal. There appears to be little difference in these properties for the cooling rates evaluated. Comparing the two 19 mm samples, W130 has a higher yield strength than W119 which can be explained by the faster cooling rate of W130. This is expected since a faster cooling rate will result in a finer microstructure and raise the yield strength. However, the average of the ultimate tensile strengths of these two samples is practically the same. Examining the ultimate tensile strength of the 6.35 mm samples, W125 has a higher value. Again this can be explained by the faster cooling rate.

It can be seen from Table 4 that, for transverse tensile tests, three of the four fractures occurred in the weld metal. The observation to be made here is that the sample with the fastest cooling rate of the four failed in the base plate. Additionally this failure was outside of the Heat Affected Zone (HAZ) indicating good mechanical properties in the HAZ. A conclusion to draw from this is that a restriction on the cooling rate may have to be made to ensure that the weld metal is as strong as the base material. A concern that has been expressed by DTNSRDC is that the filler metal which is satisfactory for HY-100 may not be satisfactory for HSLA-100 (REF. 7). It should be noted, as shown in the table, that both longitudinal and transverse tensile specimens were cut and tested. The longitudinal tensile specimen consists entirely of weld metal while the

transverse tensile specimen is a composite of weld metal, HAZ and base plate. Also by comparing the percent elongation obtained with the minimum requirement it can be seen that the weld metal meets the required value in all cases.

Impact properties are shown in Table 5 for all four weld metal samples. The Ductile to Brittle Transition Temperature (DBTT) curve for W130 is shown in Figure 19. This is the only sample for which data was available at four test temperatures. The two data points available for W119 at -60°F (-51°C) and 0°F (-17.7°C) are also plotted for comparison. Comparing the data for these two 19 mm samples, no effect of cooling rate is observed. For the 6.35 mm samples at -60°F there is a substantial difference with the faster cooler rate sample having the lowest impact energy value while the difference at 0°F is small. When comparing all of the impact data, it must be noted that the Charpy samples from the 6.35 mm welds are half size Charpy V Notch (CVN) specimens and are not required to meet the full size CVN weld metal minimum requirements. Listed at the bottom of Table 5 are the minimum values for full size CVN specimens; the impact properties of the weld metal meet the minimum requirements.

B. MICROHARDNESS TRAVERSES

Figures 20 through 23 show the results of the Vickers microhardness traverses. The comparison of the heat input rate, cooling rate and specimen thickness with the resulting hardness readings in the weld metal is as expected recognizing that the higher hardness value should correlate with the faster cooling rate.

Table 6 is a listing of the cooling rate, average hardness and standard deviation for each sample.

On each traverse plot there are regions where large fluctuations in hardness occur over small distances. For example, in Figure 21 at a distance of 2.75 mm from the chosen start point the hardness is 290 HV while at 3.00 mm a 255 HV hardness exists and at 3.25 mm the hardness is 297 HV. The reason for this could not be determined metallographically. The reason may be due to chemical inhomogeneity and segregation in the weld metal.

In correlating the average hardness with yield strength, the 19 mm sample results are as expected. The harder the material the higher the yield strength. However, yield strengths for the 6.35 mm samples are at variance to expected results. The unexpected data point is the 113 ksi value for W123. The ultimate tensile strength of the 6.35 mm samples is in agreement with expected values. This leads to the conclusion that two test points are probably not sufficient to accurately determine the average yield strength because in the welds a large amount of scatter is expected. If more tests were performed it is expected that the value for the yield strength for the slower cooling rate sample would be lower than the yield strength value for the sample with the faster cooling rate.

C. METALLOGRAPHY

The solidification structure for each specimen is shown in Figures 24 through 27. All welds have a solidification structure that is cellular dendritic.

The microstructure as observed by optical microscopy is shown in Figures 28 through 31. All welds show a similar microstructure made up primarily of

acicular ferrite with some polygonal ferrite interspersed. Regions of side plate ferrite can be seen in small amounts and in localized regions. However, in general it is very difficult to distinguish any differences in microstructure resulting from the different cooling rates. Therefore, only microstructures representative of the high, middle and low hardness regions in all welds are shown. Next to each of the optical micrographs is a scanning electron microscope (SEM) micrograph. These micrographs were taken of the same regions as the optical micrographs in order to help reveal any differences. However, little difference could be seen between the regions at this or even higher magnifications of the SEM. In general it can be safely stated that the microstructure is similar throughout the welds for similar Vickers hardness values.

Figure 31 (a) (330 HV) shows a microstructure made up of acicular ferrite primarily but clearly illustrates side plate ferrite that has nucleated from a prior austenite grain boundary. Figure 31 (c) (216 HV) shows a coarse microstructure with areas of polygonal ferrite (PF) and dark etching areas (MAC) corresponding to regions of some combination of austenite, martensite, pearlite and carbides (Ref. 5). In Figure 31 (d) prior austenite grain boundaries can be clearly seen. These boundaries form while the weld metal is in the austenite temperature range and are the source for the nucleation of side plate ferrite.

Figures 32 through 37 were chosen to show the results of the transmission electron microscopy work. These micrographs are representative of the microstructural constituents identified in an extensive TEM investigation of the fusion line and weld metal

thin foil samples. Figure 32 (a) illustrates inclusions and interlocking laths which are characteristic of an acicular ferrite microstructure. This TEM micrograph is from the 19 mm weld metal sample with the fastest cooling rate. The average lath width for this cooling rate is listed in Table 7 along with the other cooling rates. An expected result that slower cooling rates produce wider laths can be observed. Figure 32 (b) shows the fusion line microstructure which also reveals inclusions and interlocking laths in the same micrograph.

Figures 33 (a) and (b) show the microstructure of the 6.35 mm weld metal sample with the faster cooling rate. Again the microstructure is predominately acicular ferrite with inclusions randomly interspersed throughout the microstructure. Both micrographs show the interlocking lath structure, although in Figure 33 (b) an area of seven parallel laths can be seen on the left hand side of the micrograph. It is possible that this structure is side plate ferrite.

Figure 34(a) is a TEM micrograph of the slow cooling rate 19 mm weld metal sample while Figure 34 (b) is a micrograph of the slow cooling rate 6.35 mm fusion line sample. In Figure 34 (a) the large white areas are believed to be polygonal ferrite which would be more pronounced in a slow cooling rate sample. It should be noted that the lath width appears to be larger in this micrograph which is expected for a slow cooling rate sample. In Figure 34 (b) again an inclusion can be seen while the lath size appears to have increased even more along the fusion line.

Figure 35 (a) reveals a lath structure which runs predominately in one direction. This could be side plate ferrite or upper bainite since this lath

morphology is characteristic of both. Inclusions can be identified as well as dislocations such as those in the second lath from the bottom. These dislocations are to be expected since a large part of the strength for this alloy must be due to a high dislocation density. Figure 35(b) reveals the high dislocation density and the presence of precipitates. These precipitates cannot be positively identified as to chemical composition without further investigation.

Figure 36 (a) is a micrograph of the 19 mm slow cooling rate weld metal. Two dark bands in the large polygonal ferrite grain have been determined to be microtwins. Figure 36 (b) is a dark field electron micrograph of the same region in which the microtwins appear white on the dark background. Microtwins were identified in some localized regions but were not a major microstructural constituent and thus the presence of microtwins should not be a cause for concern.

Figure 37 (a) is included to show a representative bright field micrograph of retained austenite in the weld metal. Figure 37 (b) is a representative dark field of retained austenite which happens to be along the fusion line. The retained austenite in this micrograph shows up as long narrow bands indicating that they lie between laths. Retained austenite was frequently observed to be present between the laths of ferrite.

V. DISCUSSION OF RESULTS

Acicular ferrite is the predominate microstructure in all of these welds. An acicular ferrite microstructure can be produced by austenitizing the material above 1093°C and water quenching (Ref 4). This indicates that a sufficiently fast cooling rate must be used in the welding process. This helps explain why the Submerged Arc Weld (SAW) specimens welded and tested by DTNSRDC exhibited the lowest tensile properties. This suggests more restrictive heat input/plate thickness combinations are necessary with the current consumables for SAW (Ref. 7) in order to produce acceptable strength levels.

The actual mechanisms by which acicular ferrite is produced is quite complex although general observations can be made. Abson and Dolby (Ref. 8) reported the observation that laths of acicular ferrite nucleate independently and grow steadily to mutual impingement. Figures 33 (a) and (b) show the results of this mechanism. Ricks, Howell and Barrite (Ref. 9) observed that acicular ferrite is comprised of intragranularly-nucleated Widmanstatten ferrite. In other words acicular ferrite is Widmanstatten ferrite in a uniformly fined grained microstructure which the laths have no particular orientation (interlocking). This intragranular transformation is affected by the cooling rate and the inclusion content of the weld. It is easy to understand that cooling rate can be controlled in a welding process. However, inclusion content is worthy of further investigation.

One of the major sources of inclusions in weld metal is oxides. Therefore all welding processes exclude oxygen from the weld metal as much as possible by a flux covering or an inert gas. The later method is used in the GMAW process. However, there are still some oxides formed. It is believed the inclusions which are shown in the TEM micrographs are these oxides. Harrison and Farrar (Ref. 10) report that reducing the oxygen content changed the microstructure from acicular ferrite to parallel lath ferrite (Widmanstatten ferrite has the same morphology). This marked microstructural change suggests that these small oxidation products may be of fundamental importance to the nucleation of acicular ferrite (Ref. 10). As previously mentioned Abson and Dolby investigated the effects of oxygen content on the formation of acicular ferrite and found weld metal with low oxygen content produced side plate ferrite and bainite as the major microstructural constituents as shown in Figure 38 (a). They also reported that a high oxygen content produced a microstructure whose predominate constituents are side plate ferrite and intragranular plates as shown in Figure 38 (b). However, since the predominate microstructure observed in this thesis research was acicular ferrite it appears that the GMAW process falls into Abson and Dolby's intermediate oxygen regime. Figure 38 (c) shows that a predominately acicular ferrite microstructure with some bainite and side plate ferrite can be achieved with the proper cooling rate. All of these microstructures have been observed in this research [review Figures 31 (a), (b) and 35 (a)]. Figure 38 (d) shows a schematic CCT diagram reported by Glover (Ref. 5) and used by Abson and Dolby to evaluate the influence of cooling rate on microstructure.

Decreasing the cooling rate (line 1) would be expected to increase the tendency to form grain boundary ferrite. Therefore reviewing the micrographs, Figure 31 (a), a slow cooling rate specimen, shows grain boundary ferrite clearly while Figure 31 (a) through (f), a fast cooling rate sample, does not indicate this type of ferrite on any of the micrographs. On the other hand, increasing the cooling rate produces acicular ferrite; which is apparent in the micrographs also.

It is known that the finer the grain size the more resistent the material is to brittle fracture. This translates into a lower DBTT for a fine grained material. Therefore the data should reflect higher impact energies for the faster cooling rate samples. This is the case for the 19mm samples. There should be a correlation between hardness and cooling rate with the hardest material resulting from the fastest cooling rates. Table 6 shows this is true when taking into account scatter as shown by the standard deviation. It is interesting to note that the results of tempering can be seen in the microhardness traverse of W130. The tempered weld passes were softer than the untempered passes, Figure 21. The region to the right of the start point shows the untempered weld pass hardness values.

The retained austenite observed throughout all the samples is believed to be stable due to the partitioning of alloying elements such as Ni and Mn to the austenite during the decomposition of austenite to ferrite and carbides. This retained austenite may be important in improving fracture toughness and even resistance to hydrogen assisted cracking.

VI. CONCLUSIONS

1. The predominate microstructure for all four cooling rates was acicular ferrite.

2. For the slower cooling rate samples a small amount of side plate ferrite was observed.

3. The role of inclusions in the formation of intragranular acicular ferrite was observed.

4. The GMAW process provided the proper amount of oxides to serve as inclusions for the intragranular nucleation of acicular ferrite.

5. The GMAW weld mechanical properties meet or exceed all the required minimum values.

6. Retained austenite was observed and believed to be stable.

7. Dark etching areas were observed by optical microscoscopy to correspond to soft regions (250 HV and below), however the microconstituents could not be identified.

8. The tensile test results of three samples failing in the weld metal indicate that in these cases the weld metal had not been strengthened to the base metal strength. It is possible that cooling rate restrictions will have to be applied to the 120-S filler metal if the weld metal is to be stronger than the HSLA-100 base-metal.

VII. RECOMMENDATIONS

Although the predominate microstructure was acicular ferrite the chemical composition of the resulting microstructure does not appear to allow the weld metal to meet or exceed base metal strength at the slower cooling rates. It is therefore recommended that research and development of new filler metals for HSLA-100 steels be performed.

APPENDIX: TABLES AND FIGURES

TABLE 1

CHEMICAL COMPOSITION OF BASE PLATE, FILLER WIRE AND WELD METAL

ELEMENT	BASE PLATE (GJY) 6.35 mm	120S-1 WIRE	WELD METAL GMAW (W123)
Carbon	0.037	0.07	0.056
Manganese	0.78	1.54	1.20
Silicon	0.27	0.36	0.31
Phosphorus	0.013	0.007	0.006
Sulfur	0.002	0.005	0.006
Nickel	3.17	2.28	2.45
Molybdenum	0.62	0.47	0.53
Chromium	0.56	0.29	0.38
Vanadium	0.006	<0.01	0.006
Aluminum	0.024	0.02	0.014
Titanium	0.002	<0.01	0.006
Copper	1.36	0.01	0.53
Zirconium	<.001	0.01	0.007
Nitrogen	0.014		0.010
Oxygen	0.0034		0.027
Boron	0.001		0.003

TABLE 2

TENSILE PROPERTIES
OF THE BASE MATERIAL

ID #	LOCATION	YS 2% OFFSET KSI (MPa)	UTS KSI (MPa)	EL (%)	RA (%)
GJY	TOP	127	128	22	50
1/4"	TOP	129	130	23	53
6.35mm	BOTTOM	114	121	26	62
	BOTTOM	124	125	22	57
AVE.	******	123.5 (851.5)	126 (869)	23.3	55.5
GJX 3/4" 19mm	TOP	111 (765)	134 (924)	22	75

TABLE 3

WELDING CONDITIONS FOR HSLA-100 WELDMENTS

IDENTI-FICATION (NUMBER)	PLATE THICKNESS INCH (mm)	PREHEAT/ INTERPASS TEMP °F (°C)	HEAT INPUT kJ/IN (kJ/mm)	COOLING RATE F/SEC (C/sec)
W130	3/4 (19)	125 (51.6)	30 (1.18)	75.2 (41.7)
W119	3/4 (19)	200 (93.3)	45 (1.65)	36.7 (20.4)
W125	1/4 (6.35)	75 (23.8)	30 (1.18)	60.2 (33.4)
W123	1/4 (6.35)	125 (51.6)	30 (1.18)	39.0 (21.8)

TABLE 4

TENSILE PROPERTIES
OF THE WELD METAL

ID #	ORIENTATION (L/T)	YS 2% OFFSET KSI (MPa)	UTS KSI (MPa)	EL (%)	RA (%)
W130	L	123	130	22	58
	L	125	131	16	66
3/4in	T	*	125	BASE PLATE **	
	T	*	120	BASE PLATE **	
AVE.		124 (855)	126.5 (872)	19	62
W119	L	115	125	27	48
	L	120	129	29	66
3/4in	T	*	127	WELD METAL •	
	T	*	127	WELD METAL •	
AVE.		117.5 (810)	127 (875)	28	57
W125	L	106	142	26	60
	L	104	136	28	68
1/4in	T	*	130	WELD METAL •	
	T	*	130	WELD METAL •	
AVE.		105 (724)	134.5 (927)	27	64
W123	L	113	127	26	72
	L	104	122	29	70
1/4in	T	*	123	WELD METAL •	
	T	*	123	WELD METAL •	
AVE.		108.5 (748)	123.75 (853)	27.5	71
WELD METAL MINIMUM REQUIREMENTS		102-104	INFO	14	INFO

* Transverse tensile specimens are used to assess joint efficiency. The principal information derived is the ultimate tensile strength of the composite (weld, HAZ, and base plate) specimens.

** Fracture occurred in the base plate portion of the transverse specimen.

• Fracture occurred in the weld metal portion of the transverse specimen.

TABLE 5

IMPACT PROPERTIES
OF THE WELD METAL

ID #	COOLING RATE F/SEC (C/sec)	NOTCH LOCATION	TEST TEMP (F)	IMPACT ENERGY (FT-LB)	% SHEAR (%)
W130	75.2	WELD	-60	60	60
		WELD	-60	65	65
3/4in	(41.7)	WELD	-60	49	60
		AVE	*******	*58*	*61.6*
		WELD	0	78	85
		WELD	0	64	50
		WELD	0	76	85
		AVE	*******	*72.6*	*73.3*
W119	36.7	WELD	-60	75	45
		WELD	-60	27	30
3/4in	(20.4)	WELD	-60	51	45
		AVE	*******	*51*	*40*
		WELD	0	58	60
		WELD	0	64	65
		WELD	0	79	70
		AVE	*******	*67*	*65*
W125	60.2	WELD	-60	24	NOT
		WELD	-60	27	RECORD-
1/4in	(33.4)	WELD	-60	29	ED FOR
		AVE	*******	*26.6*	
		WELD	0	30	HALF
		WELD	0	30	SIZE
		WELD	0	38	CVN
		AVE	*******	*32.6*	
W123	39.0	WELD	-60	46	NOT
		WELD	-60	35	RECORD-
1/4in	(21.6)	WELD	-60	43	ED FOR
		AVE	*******	*41*	
		WELD	0	32	HALF
		WELD	0	38	SIZE
		WELD	0	32	CVN
		AVE	*******	*34*	
Weld Metal Minimum Requirements			-60	35	
Full Size CVN			0	60	

1. All specimens notched in T-L orientation.
2. Half size CVN values are reported for 6.35 mm weldments.

TABLE 6

COOLING RATE, MICROHARDNESS
MEAN AND STANDARD DEVIATION

WELD SAMPLE ID NO.	COOLING RATE 800-500°C °F/SEC (C/sec)	MICROHARDNESS TRAVERSE AVERAGE (HV)	STANDARD DEVIATION (HV)
W130	75.2 (41.7)	301.4	20.9
W119	36.7 (20.4)	273.1	15.2
W125	60.2 (33.4)	305.9	13.4
W123	39.0 (21.6)	285.7	20.7

TABLE 7

COOLING RATE VS. AVERAGE LATH WIDTH

WELD SAMPLE ID NO.	COOLING RATE 800-500°C °F/SEC (C/sec)	AVERAGE WIDTH OF LATHS MICRONS	NUMBER OF LATHS MEASURED
W130	75.2 (41.7)	.331	153
W119	36.7 (20.4)	.361	160
W125	60.2 (33.4)	.407	160
W123	39.0 (21.6)	.503	83

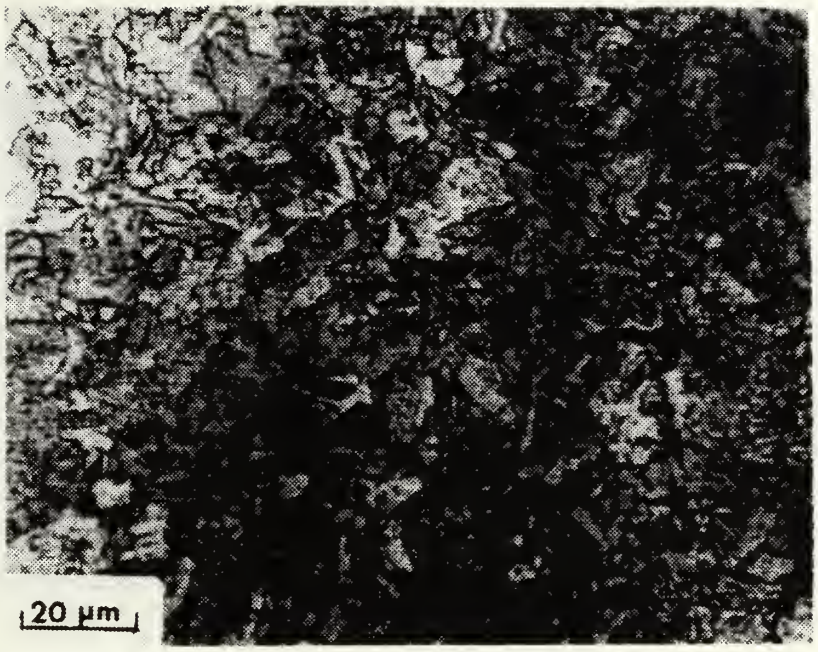

Figure 1. Optical Micrograph of W130 Base Metal

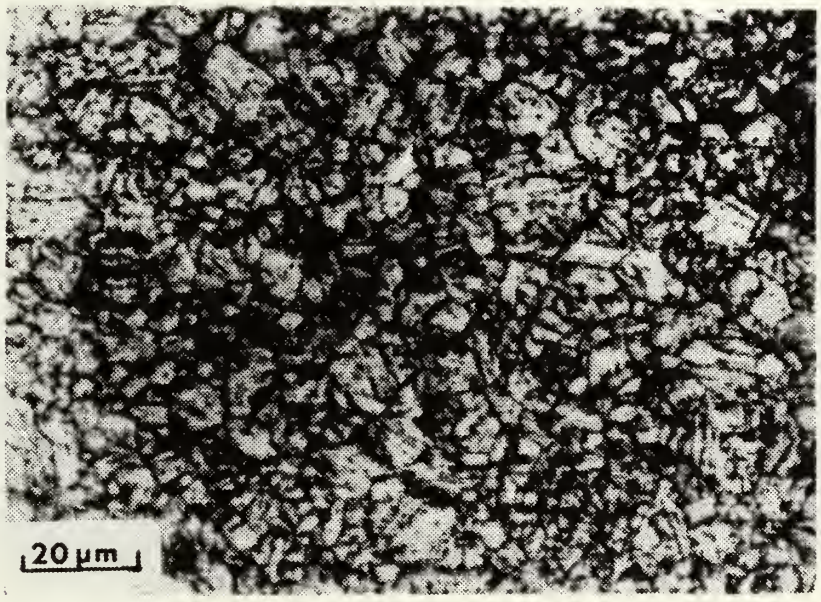

Figure 2. Optical Micrograph of W123 Base Metal

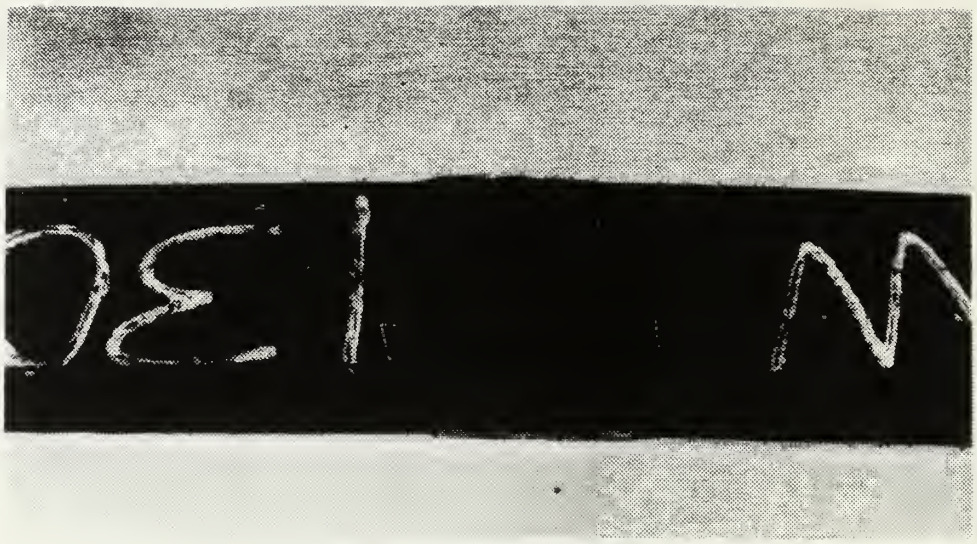

Figure 3. 19 mm Thick Plate as Received

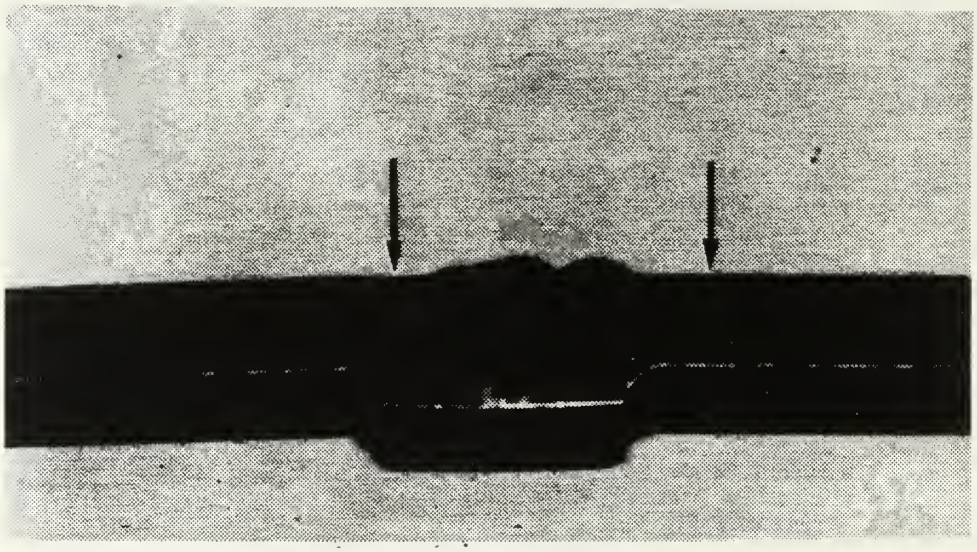

Figure 4. 19 mm Thick Plate as Received

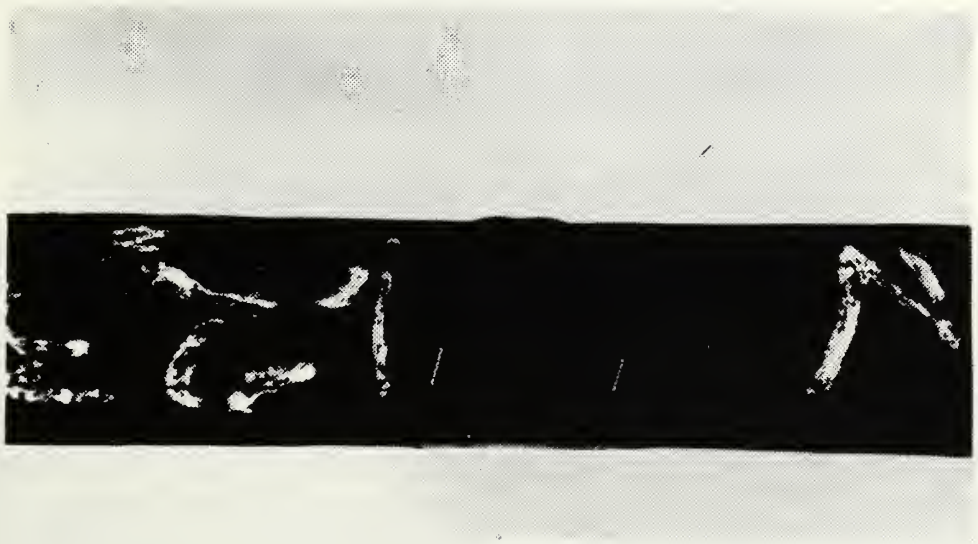

Figure 5. 6.35 mm Thick Plate as Received

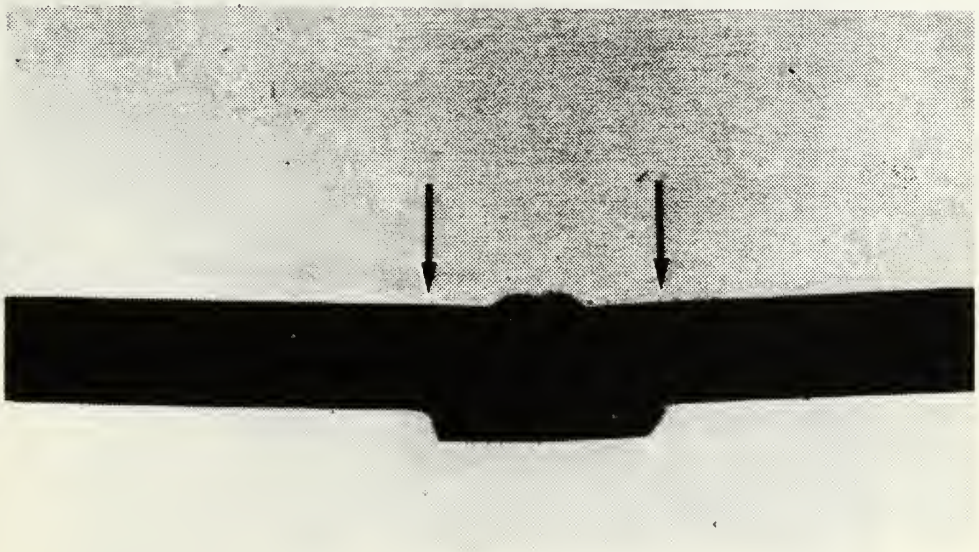

Figure 6. 6.25 mm Thick Plate as Received

Figure 7. Macroetch of W130

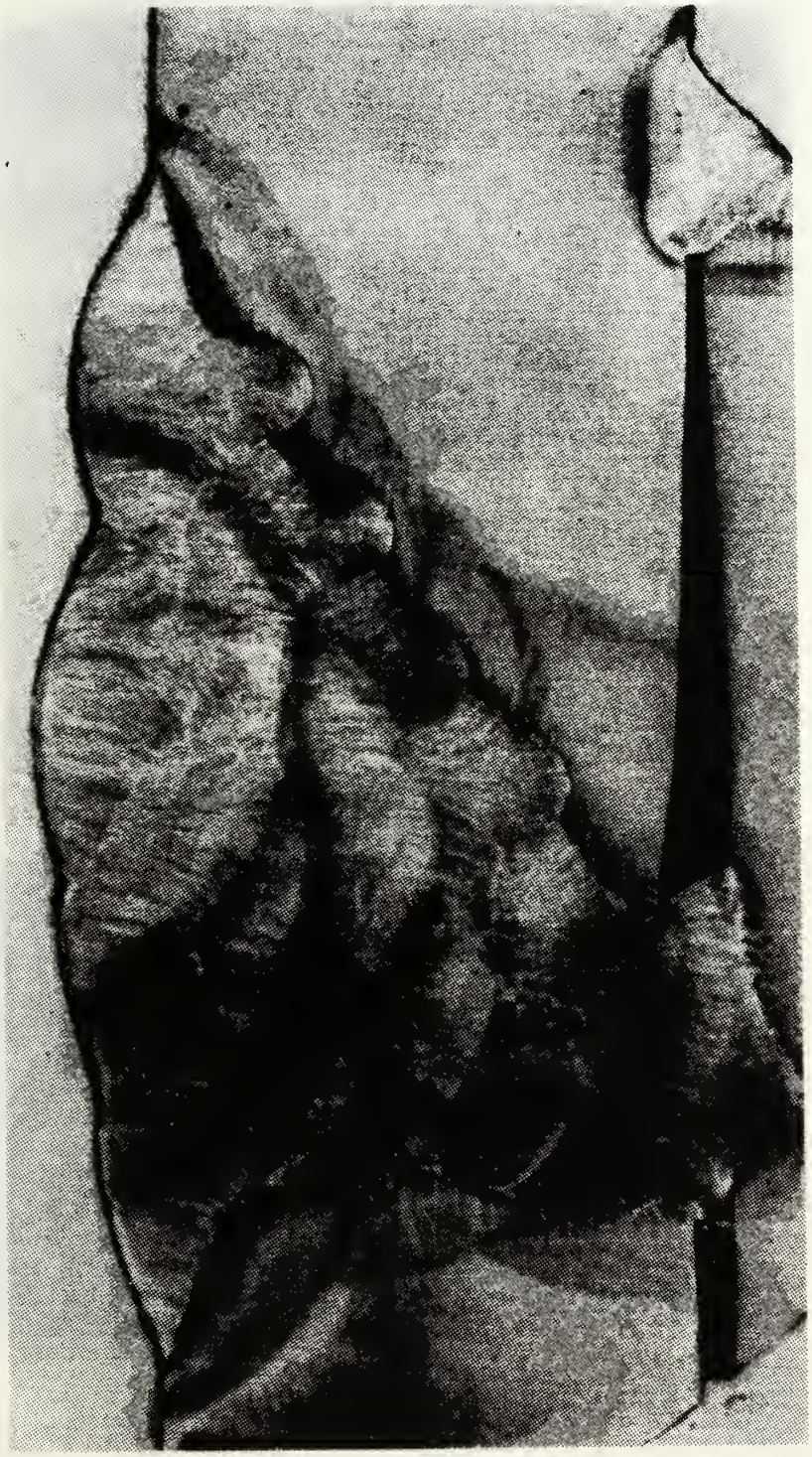

Figure 8. Macroetch of W119

Figure 9. Macroetch of W125

Figure 10. Macroetch of W123

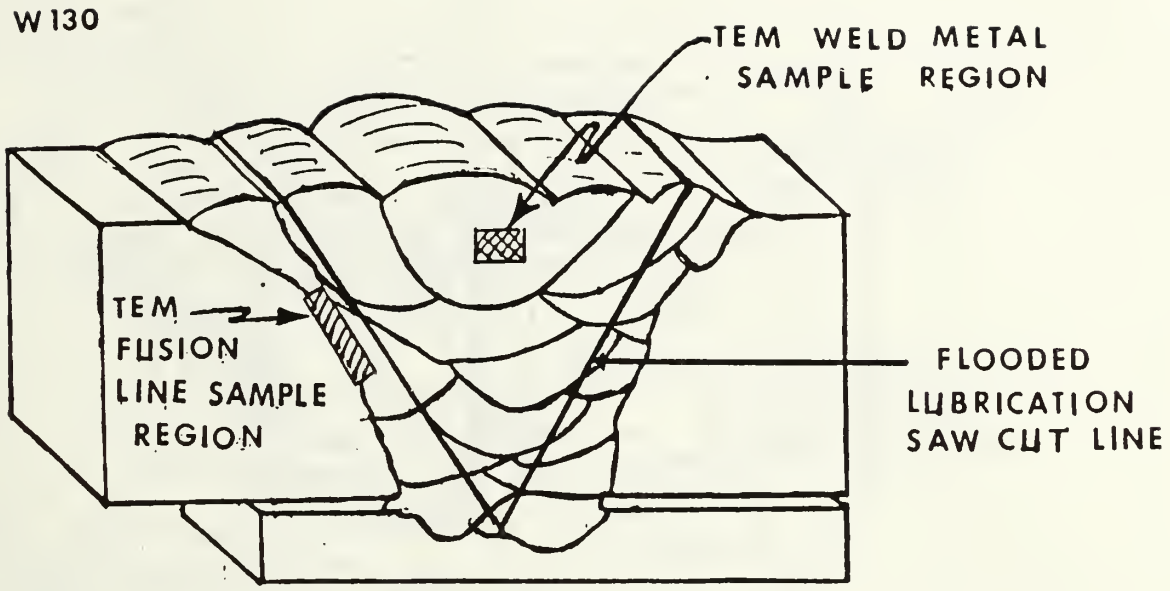

Figure 11. Three Dimensional Topography of W130

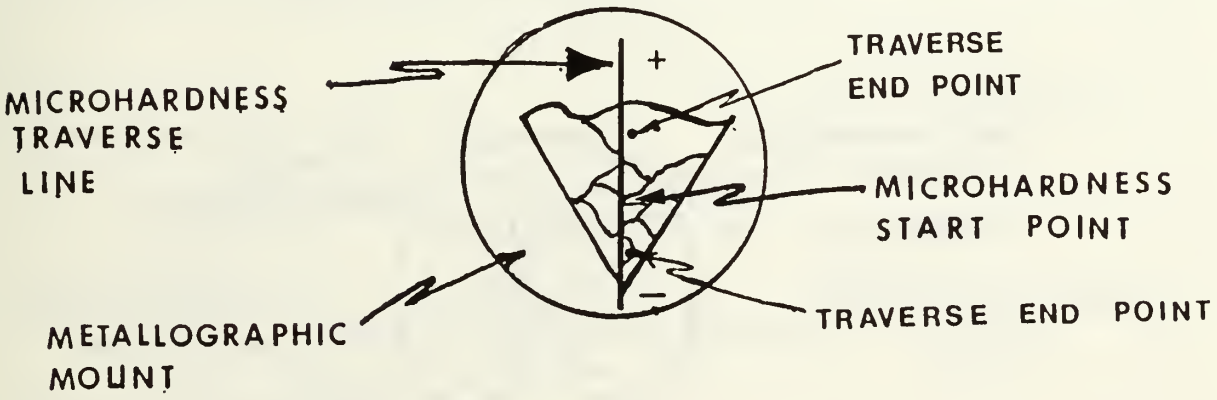

Figure 12. W130 Microhardness Traverse Sketch

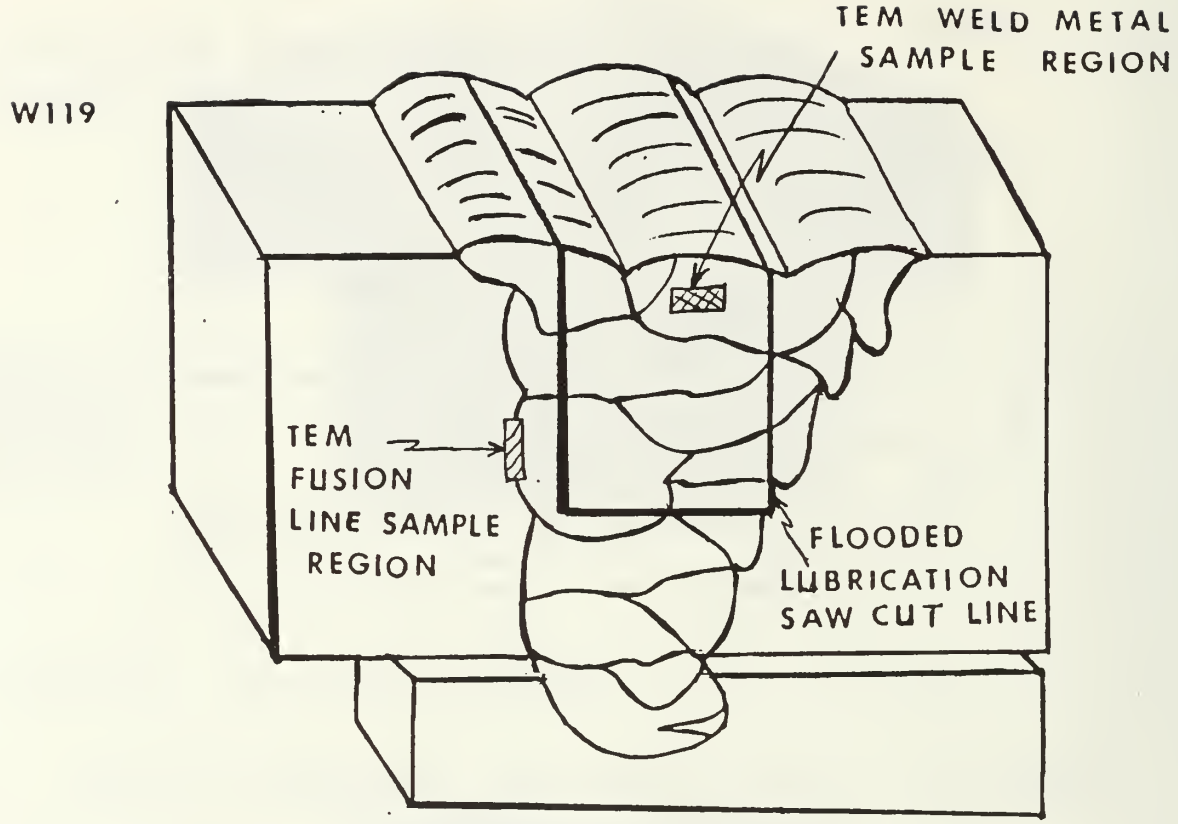

Figure 13. Three Dimensional Topography of W119

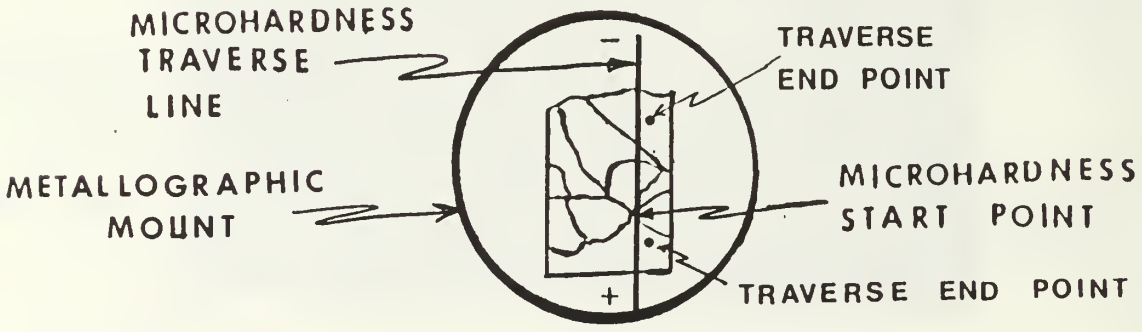

Figure 14. W119 Microhardness Traverse Sketch

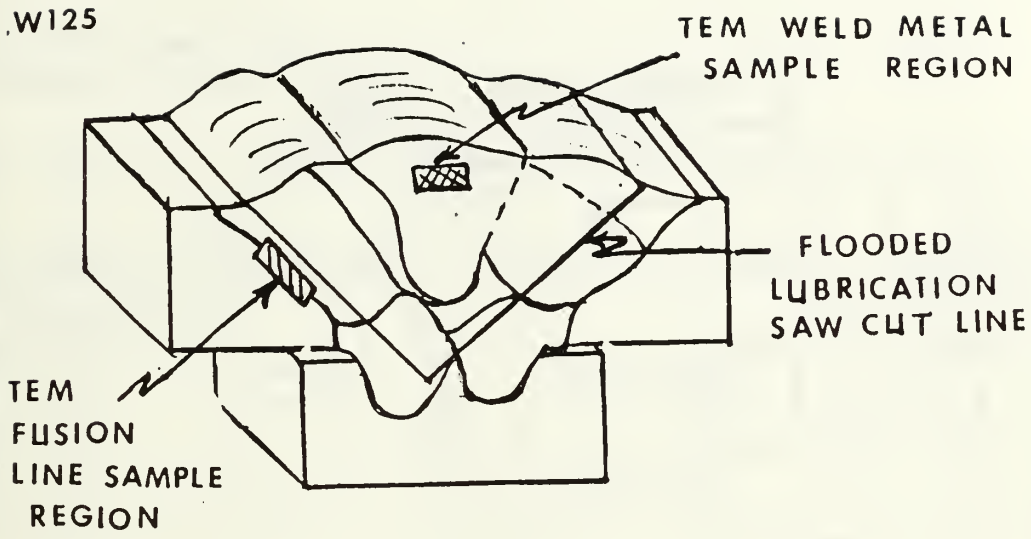

Figure 15. Three Dimensional Topography of W125

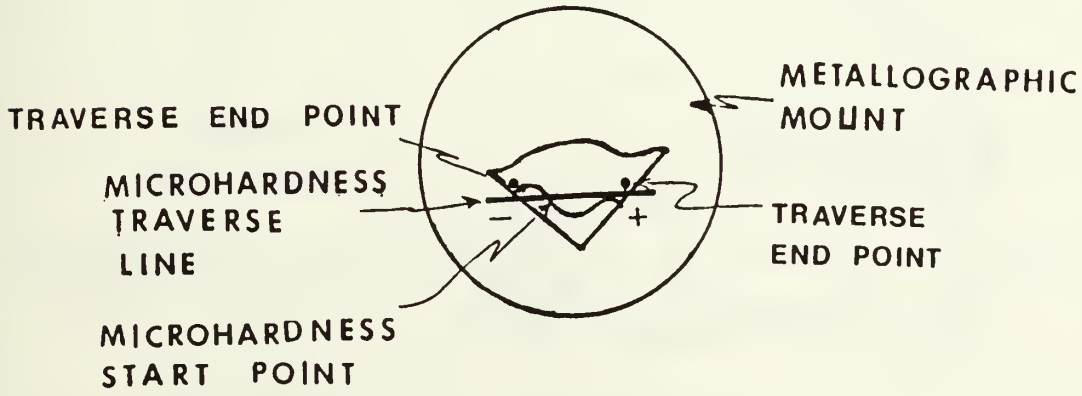

Figure 16. W125 Microhardness Traverse Sketch

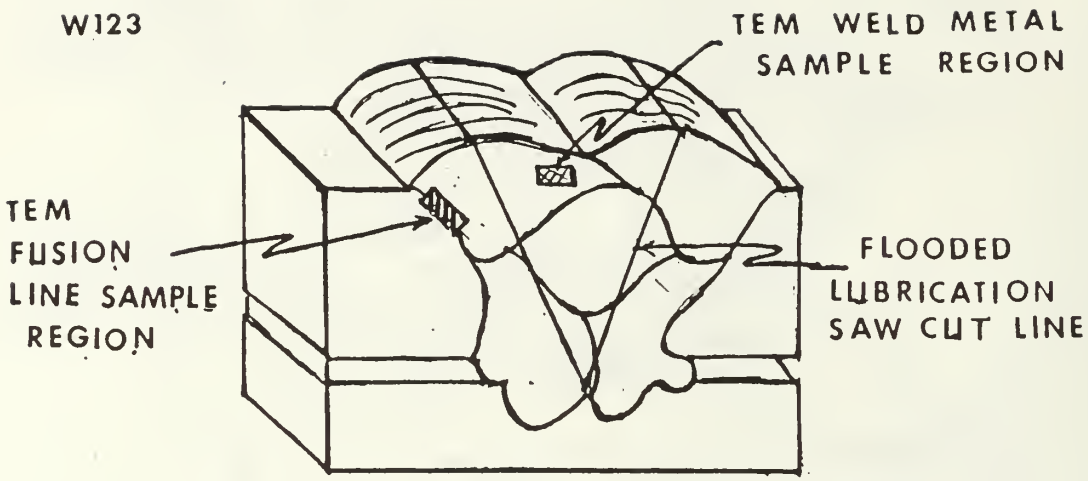

Figure 17. Three Dimensional Topography of W123

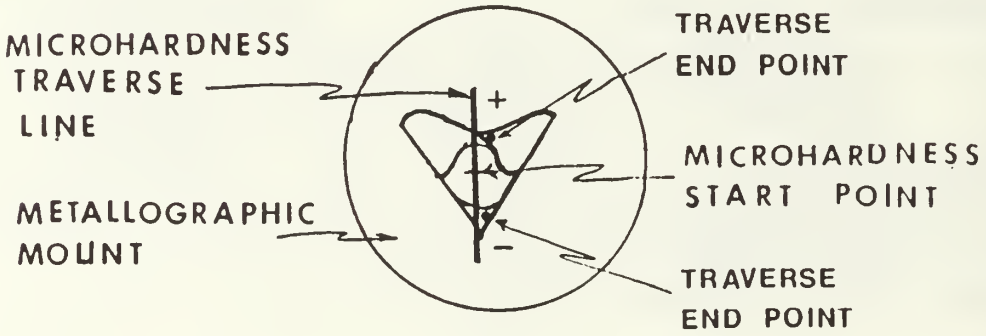

Figure 18. W123 Microhardness Traverse Sketch

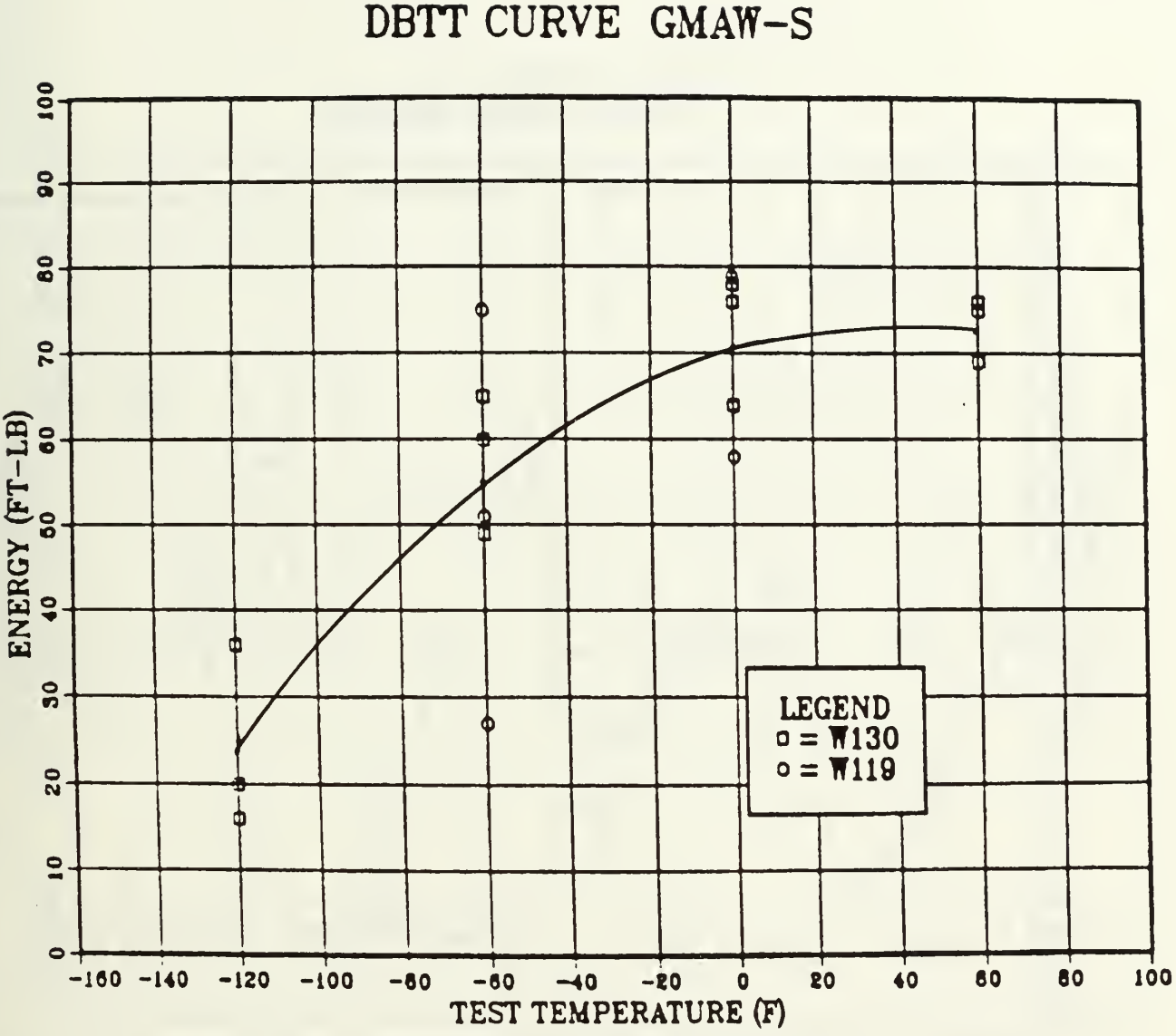

Figure 19. Ductile to Brittle Transition Curve for W130

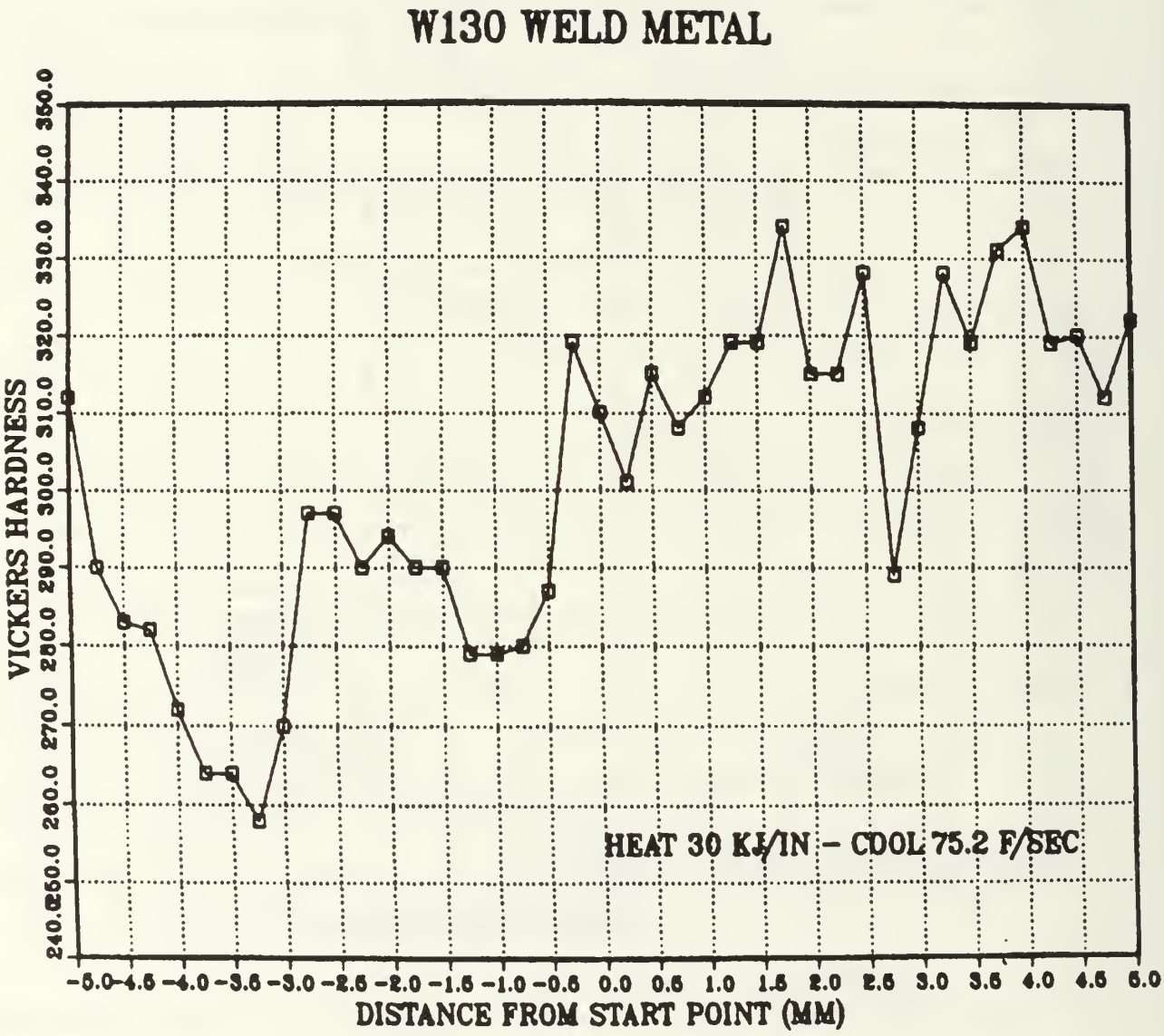

Figure 20. Vickers Hardness Traverse for W130

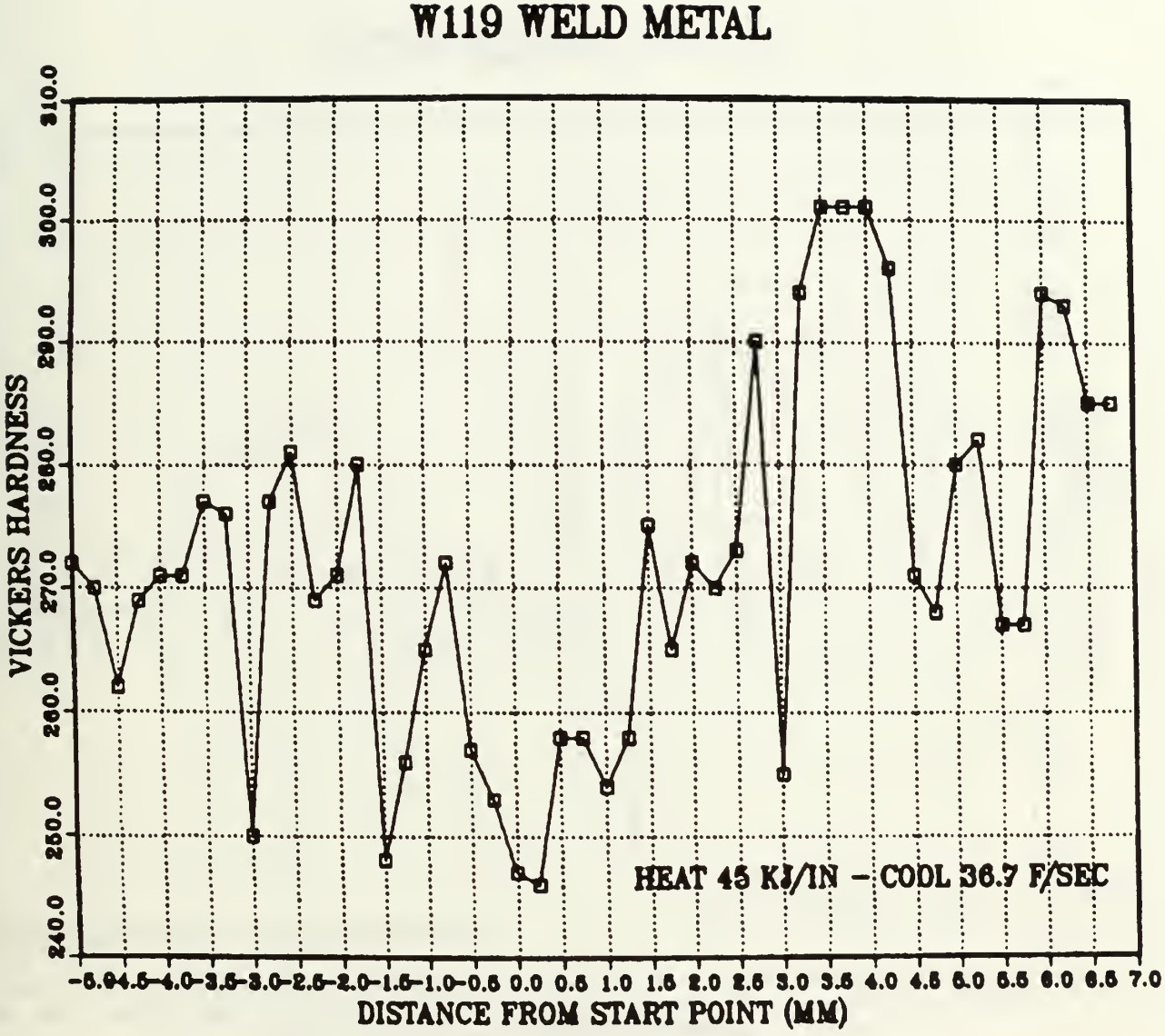

Figure 21. Vickers Hardness Traverse for W119

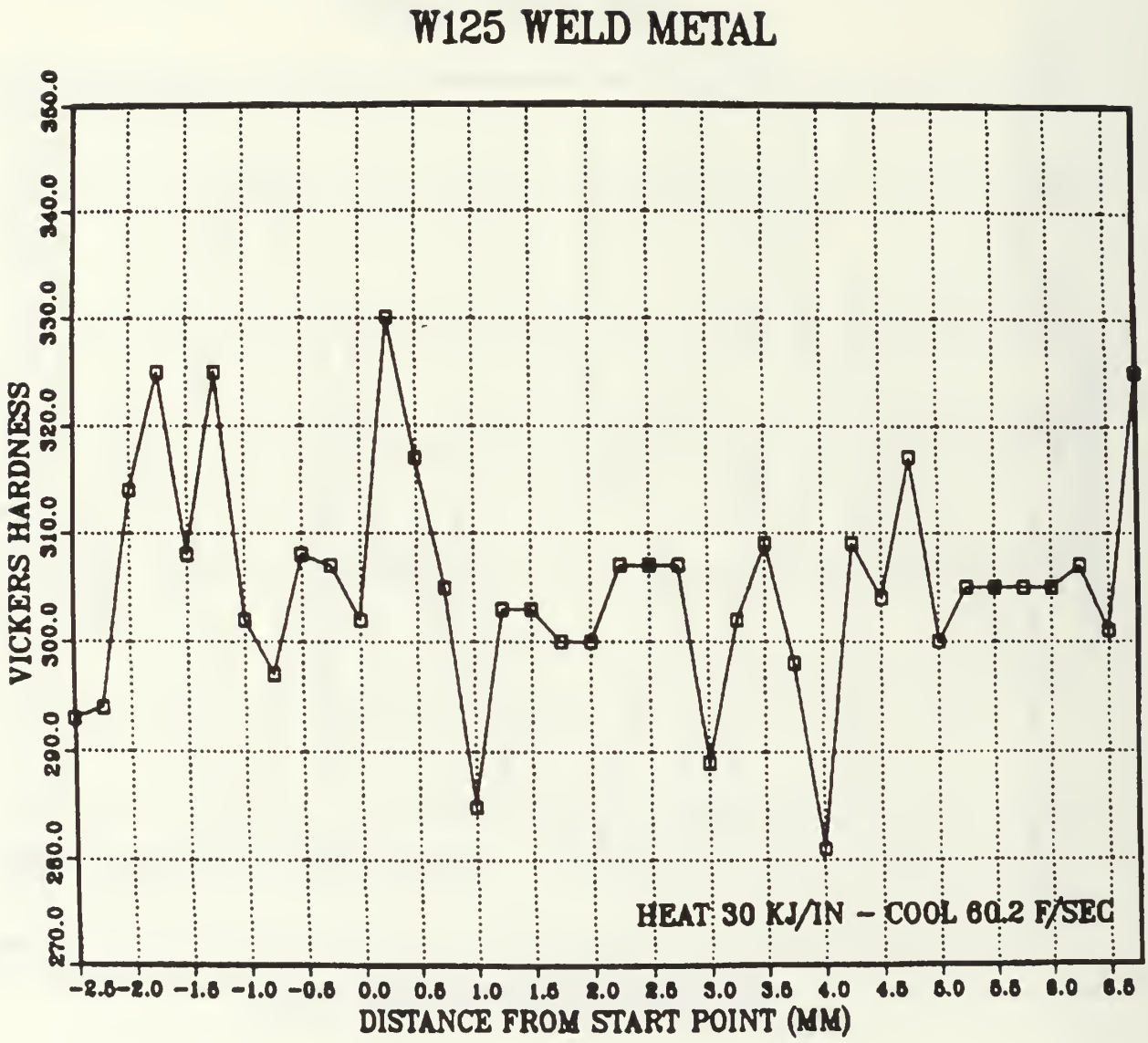

Figure 22. Vickers Hardness Traverse for W125

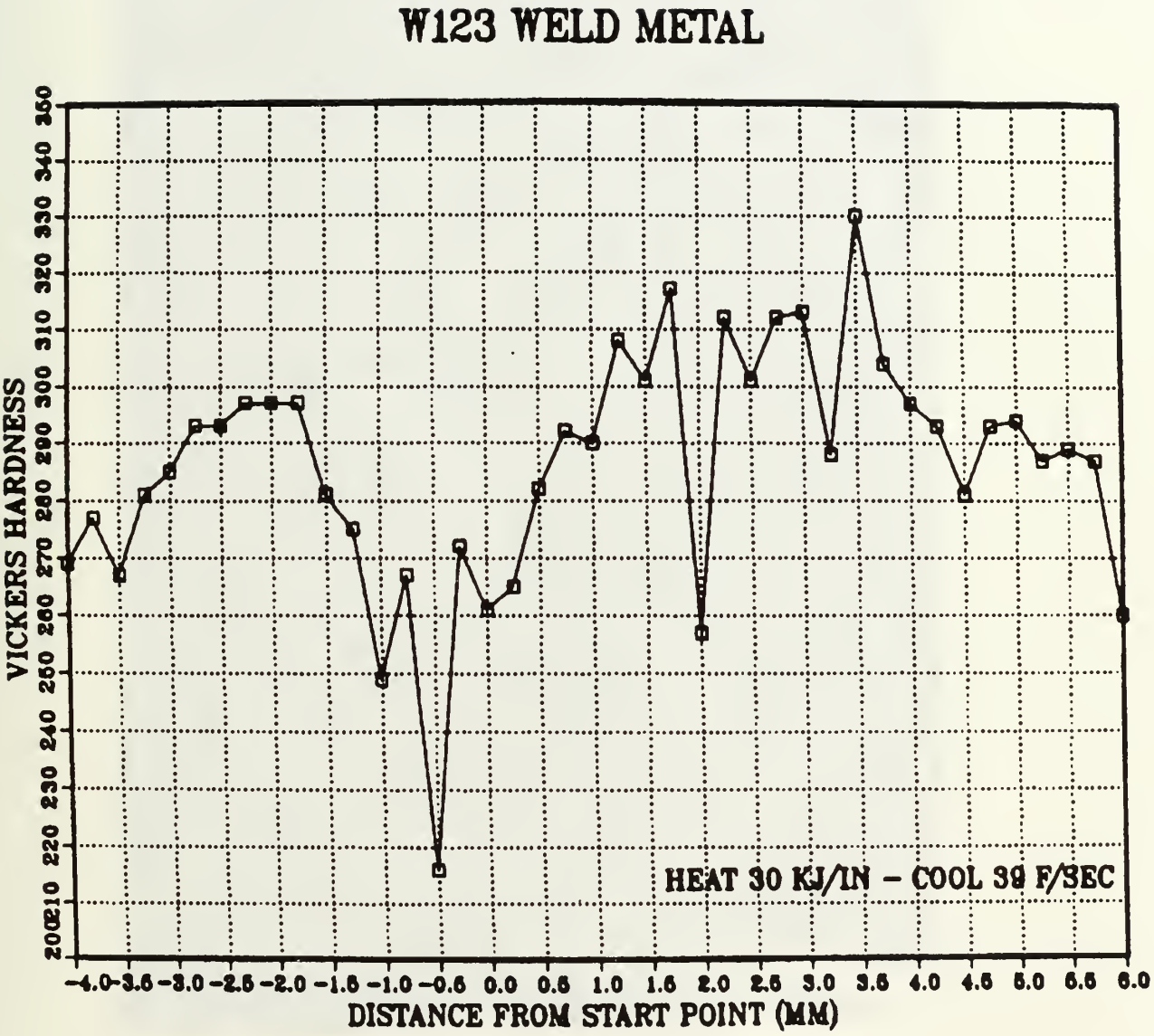

Figure 23. Vickers Hardness Traverse for W123

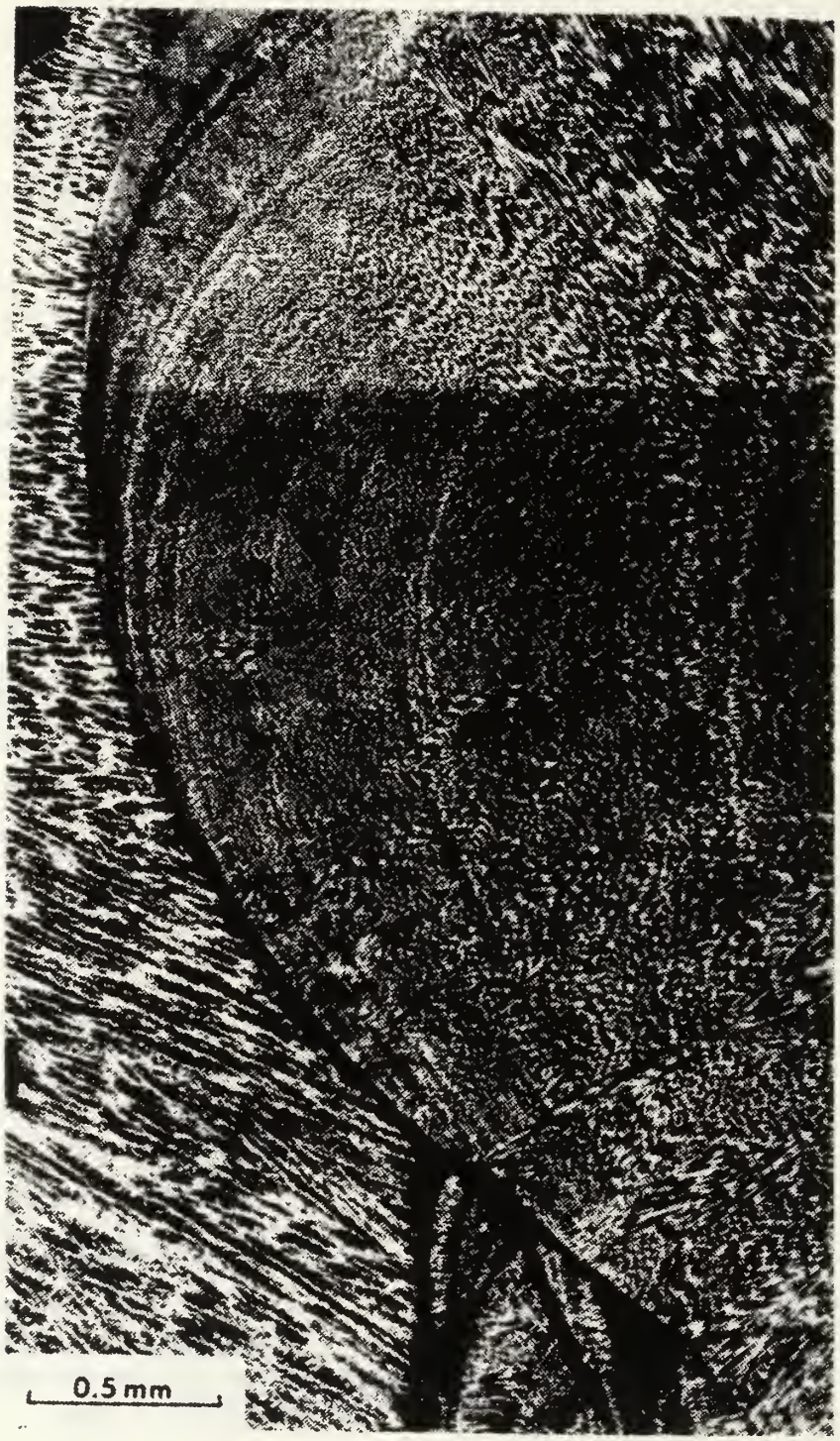

Figure 24. Solidification Structure W130

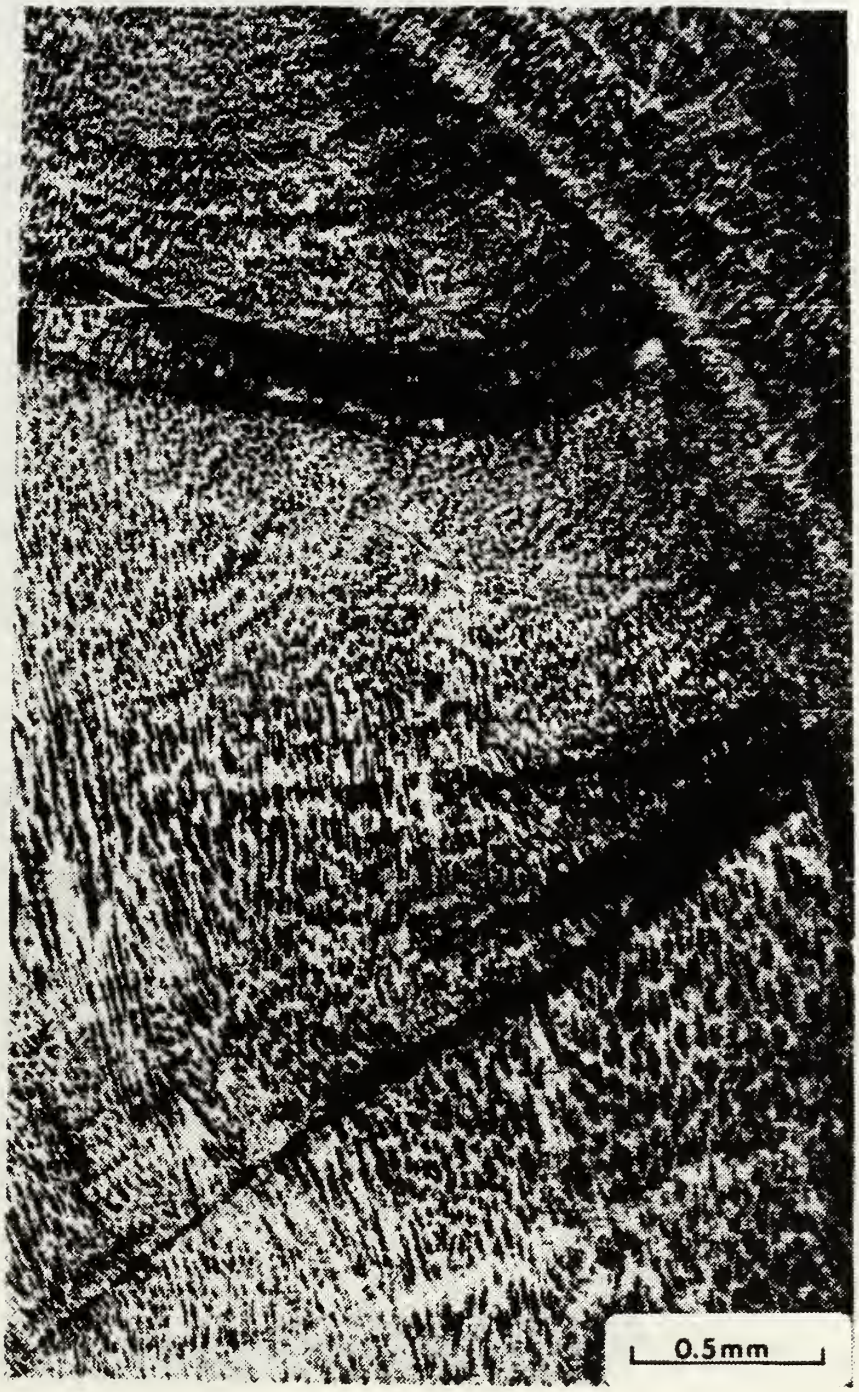

Figure 25. Solidification Structure W119

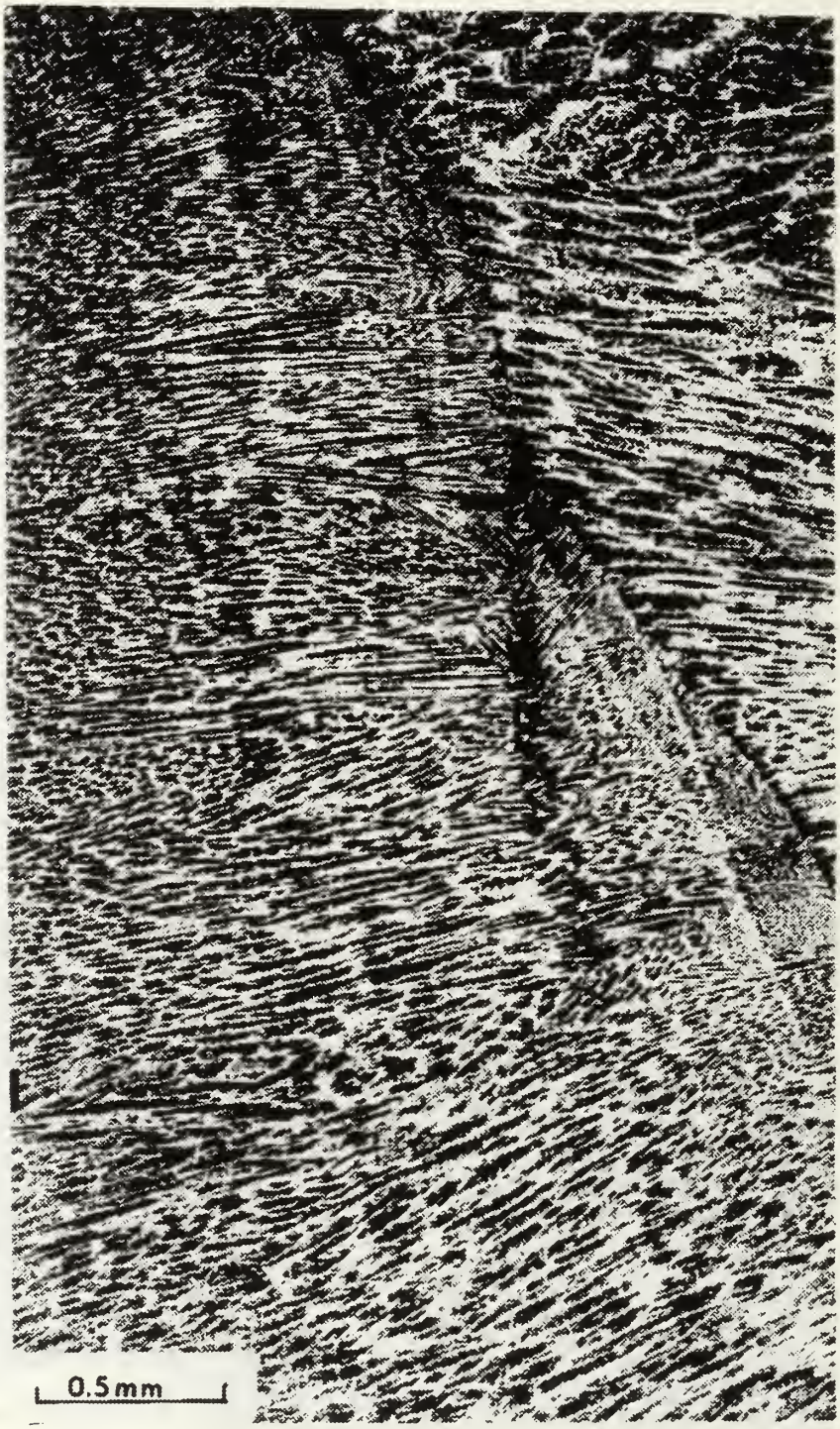

Figure 26. Solidification Structure W125

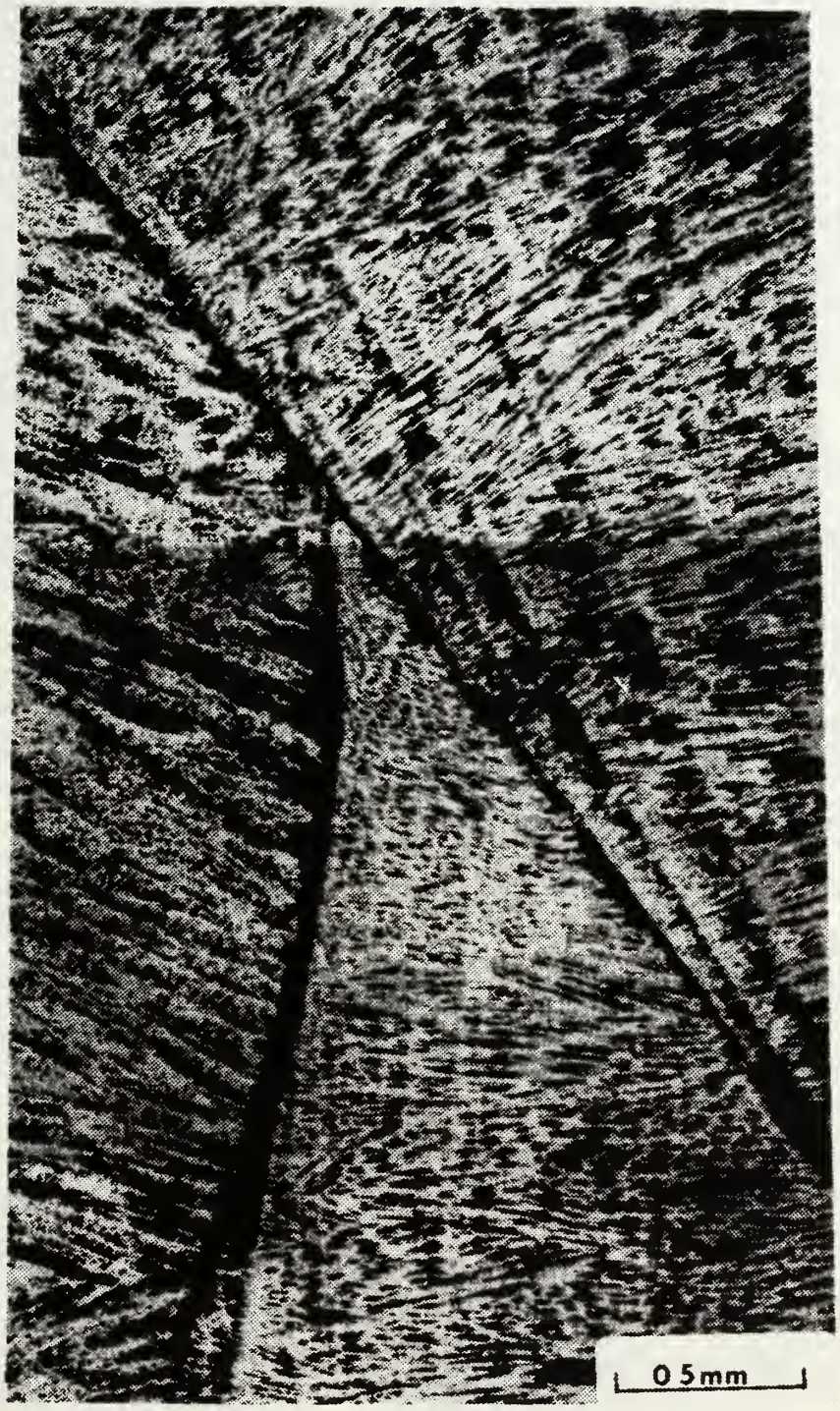

Figure 27. Solidification Structure W123

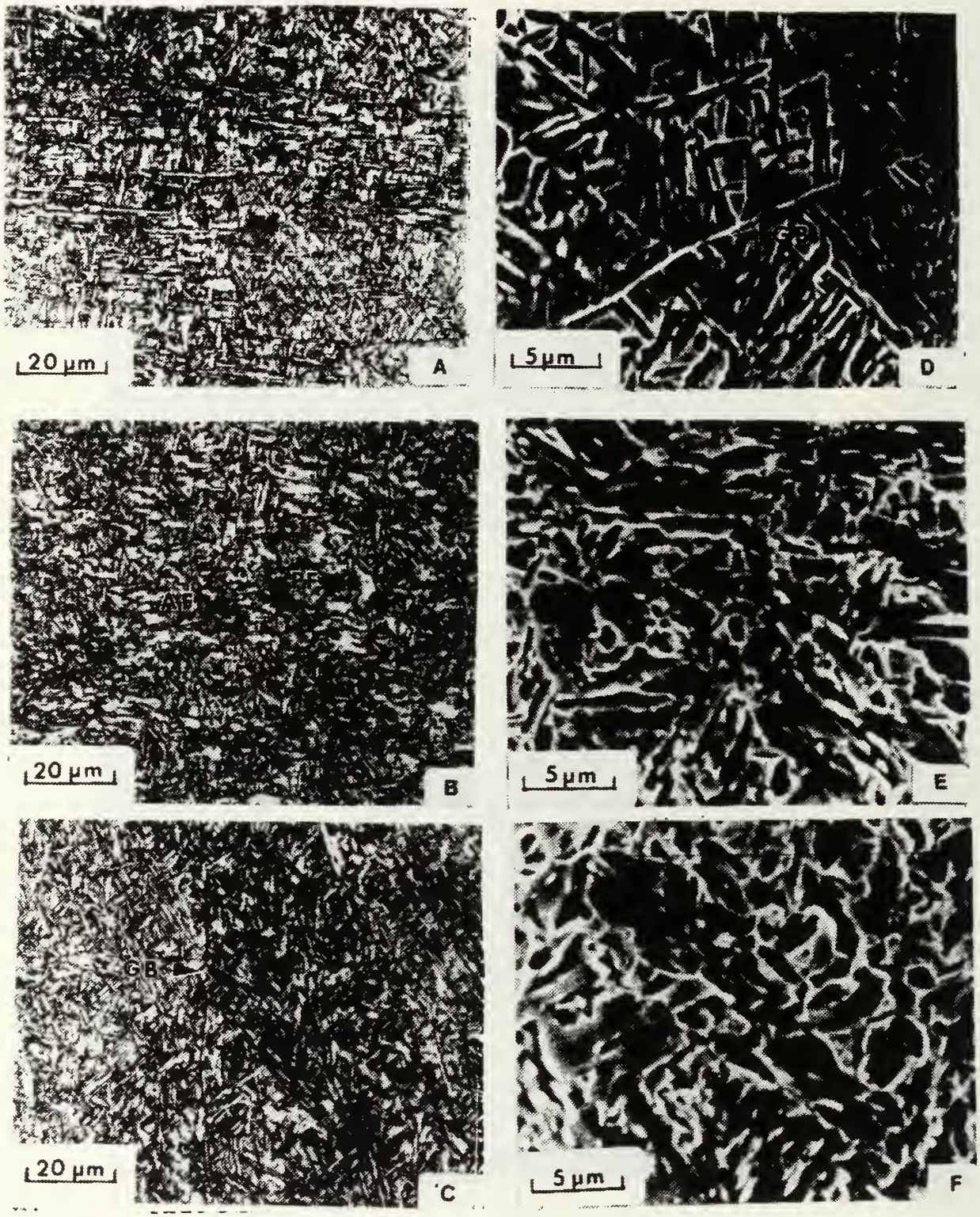

Figure 28. Micrographs of W130 (41.7°C/sec)
(A.) 334 Vickers Hardness [HV] (B.) 297 HV (C.) 258 HV
(D.) 334 HV (E.) 297 HV (F.) 258 HV

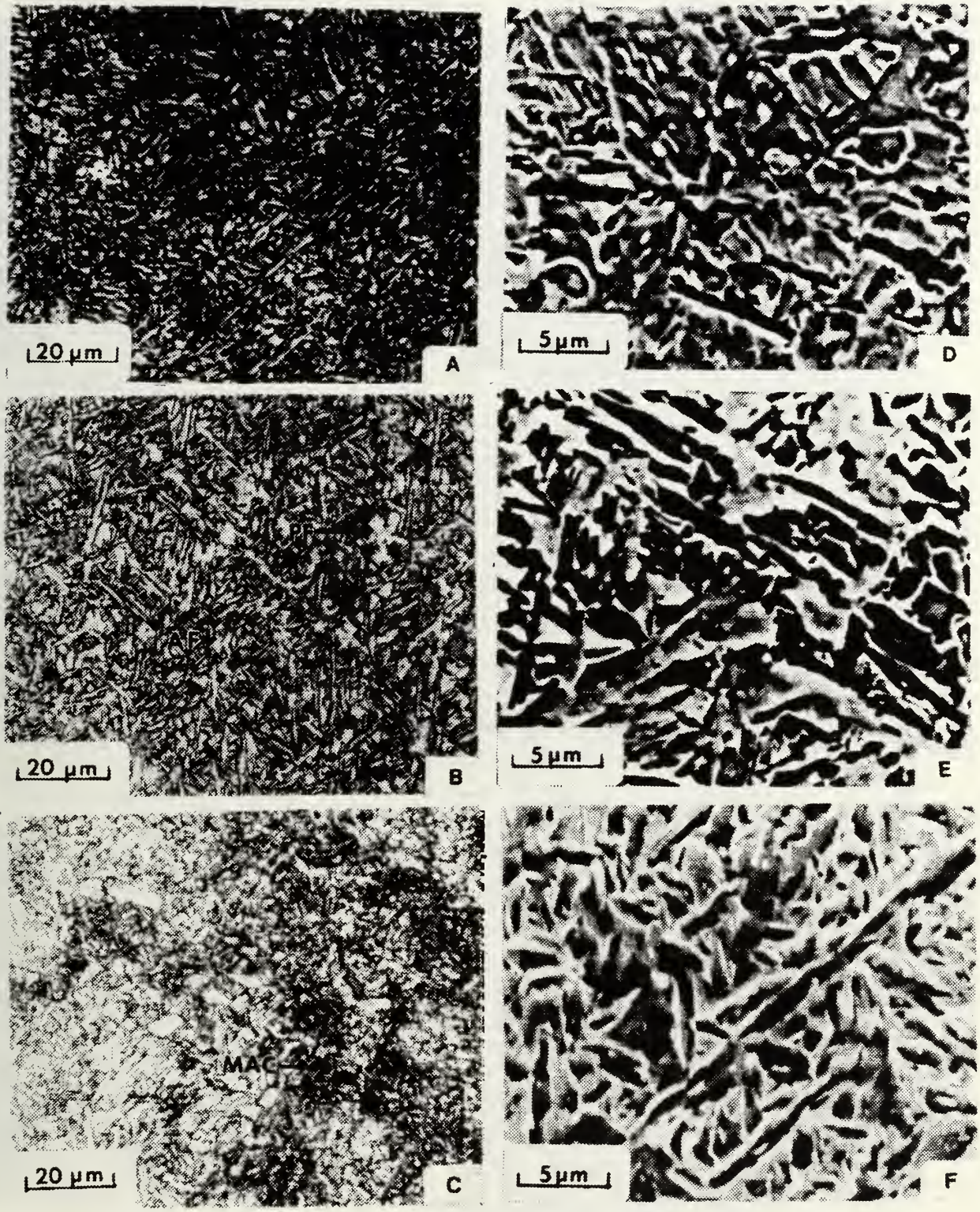

Figure 29. Micrographs of W119 (20.4°C/sec)
(A.) 301 Vickers Hardness [HV] (B.) 271 HV (C.) 265 HV
(D.) 301 HV (E.) 271 HV (F.) 265 HV

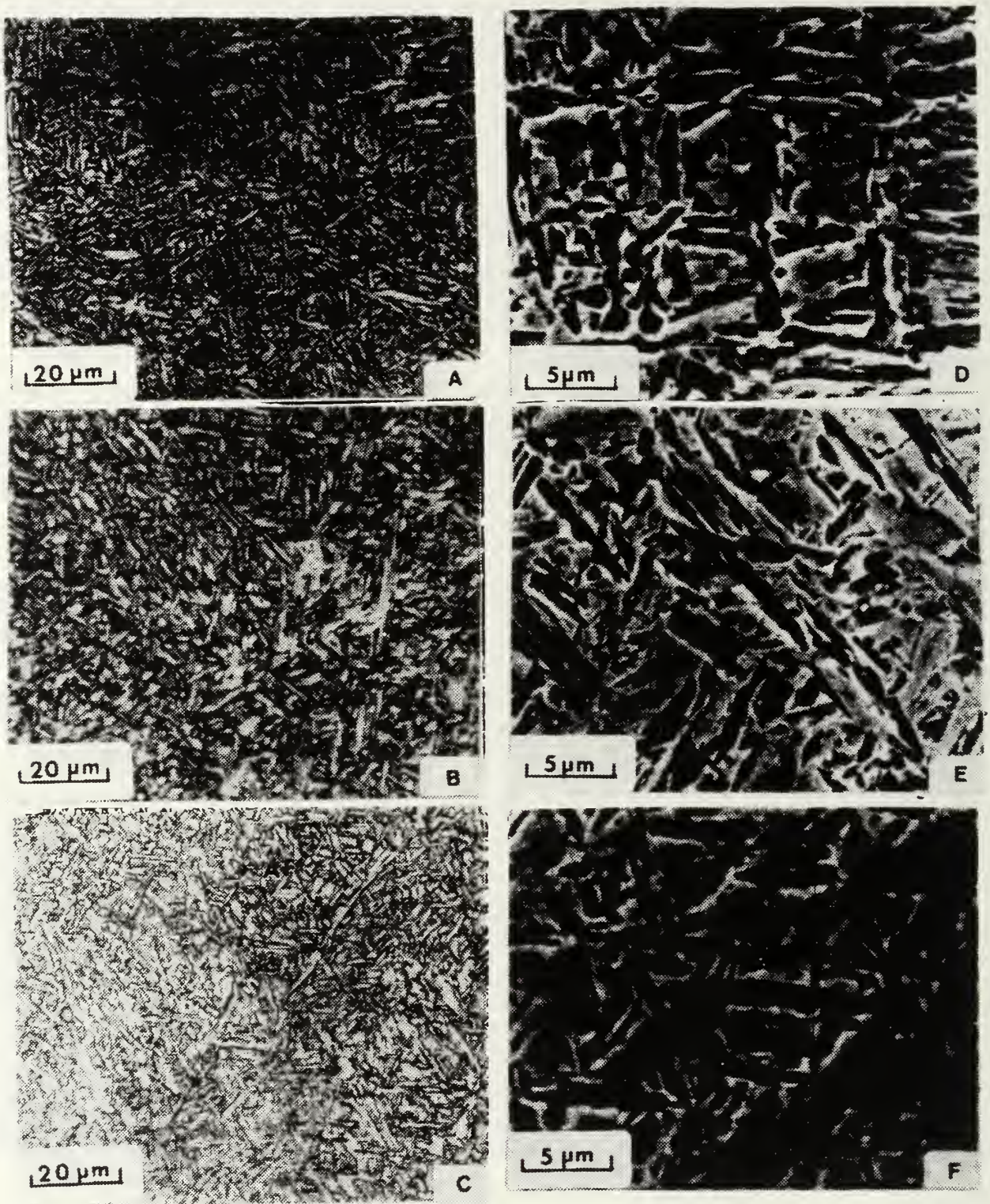

Figure 30. Micrographs of W125 (33.4°C/sec)
(A.) 327 Vickers Hardness [HV] (B.) 305 HV (C.) 297 HV
(D.) 327 HV (E.) 305 HV (F.) 297 HV

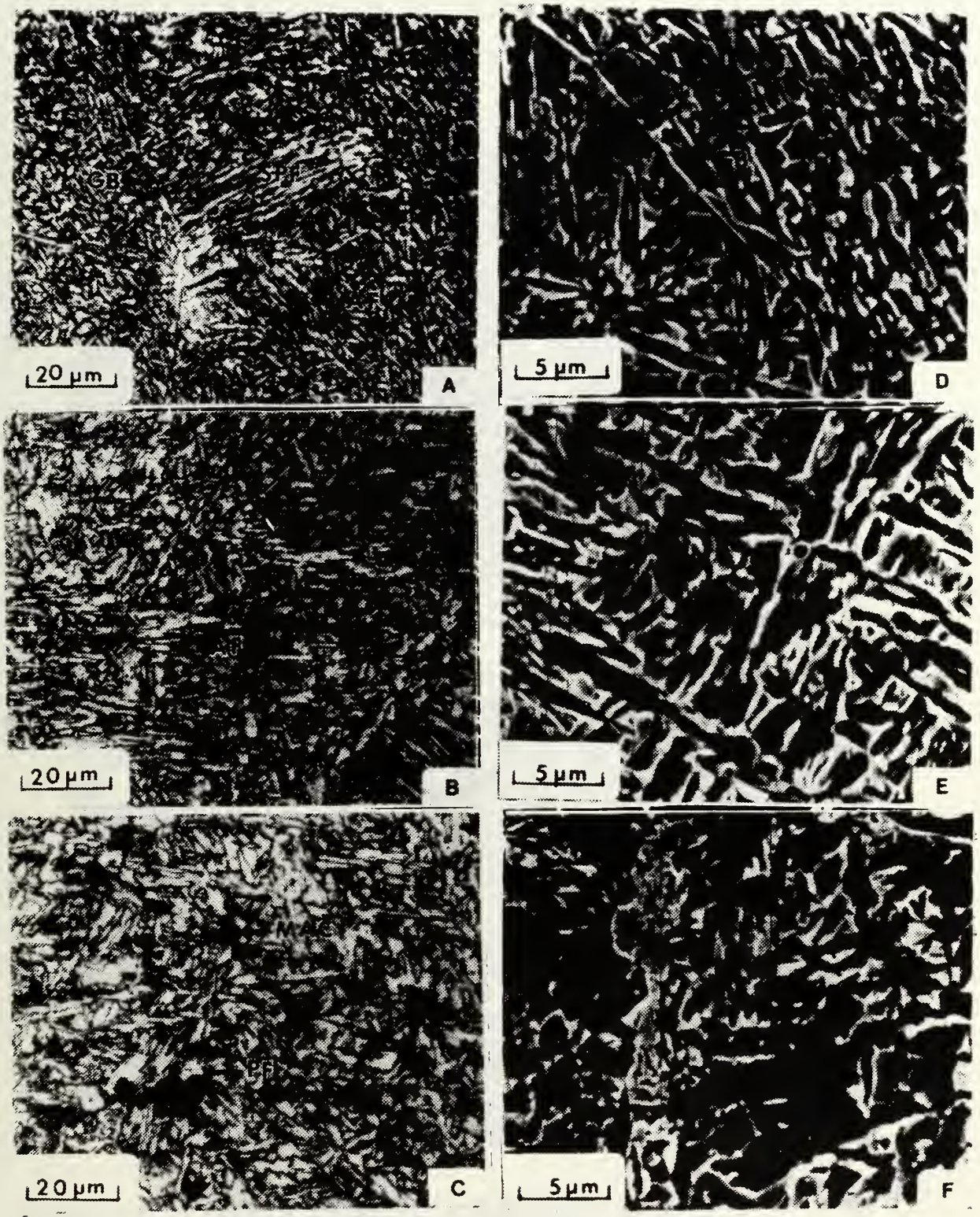

Figure 31. Micrographs of W123 (21.6°C/sec) (A.) 330 Vickers Hardness [HV] (B.) 293 HV (C.) 216 HV (D.) 330 HV (E.) 293 HV (F.) 216 HV

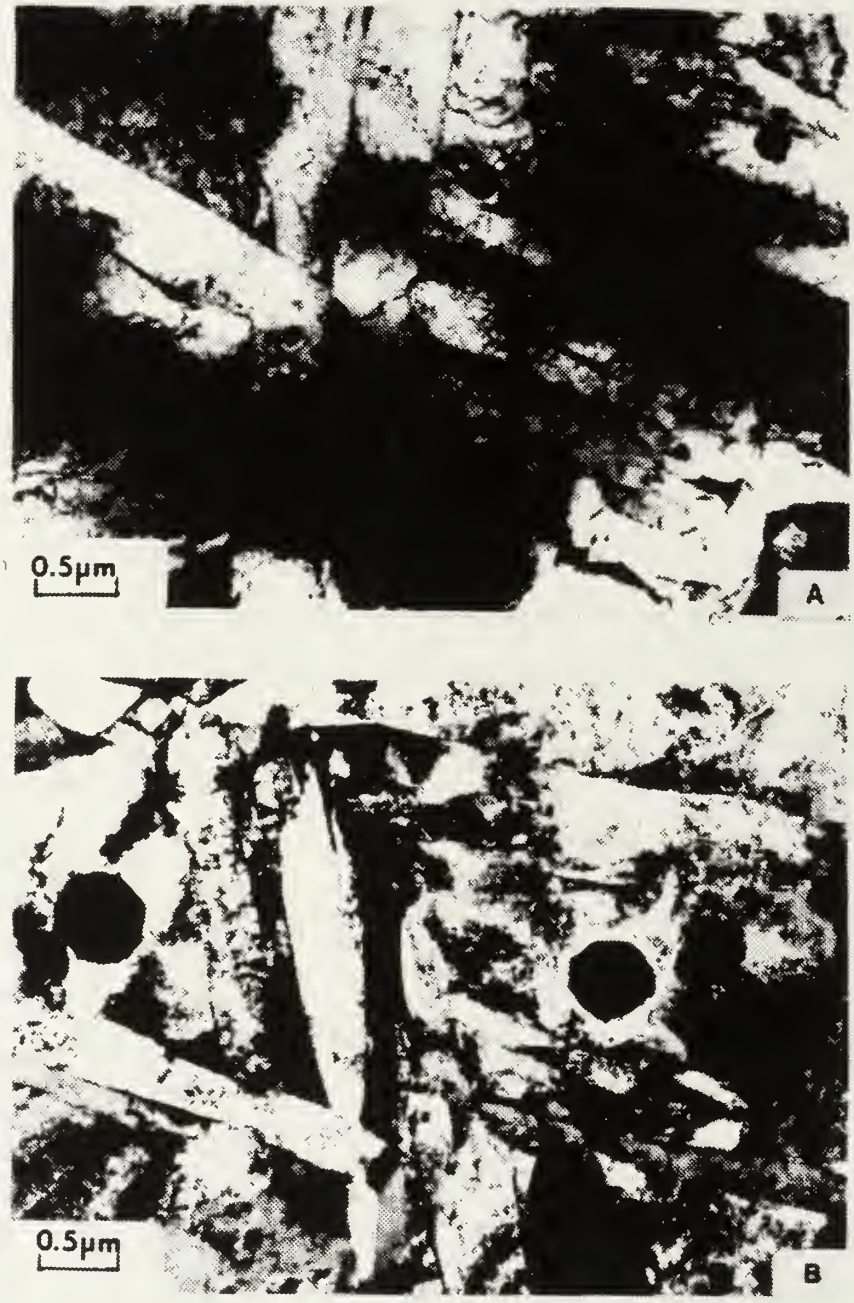

Figure 32. TEM Micrograph of W130
A.) Inclusions, Acicular Ferrite and Laths in the Weld Metal
B.) Inclusions and Laths in Fusion Line Thin Foil Sample

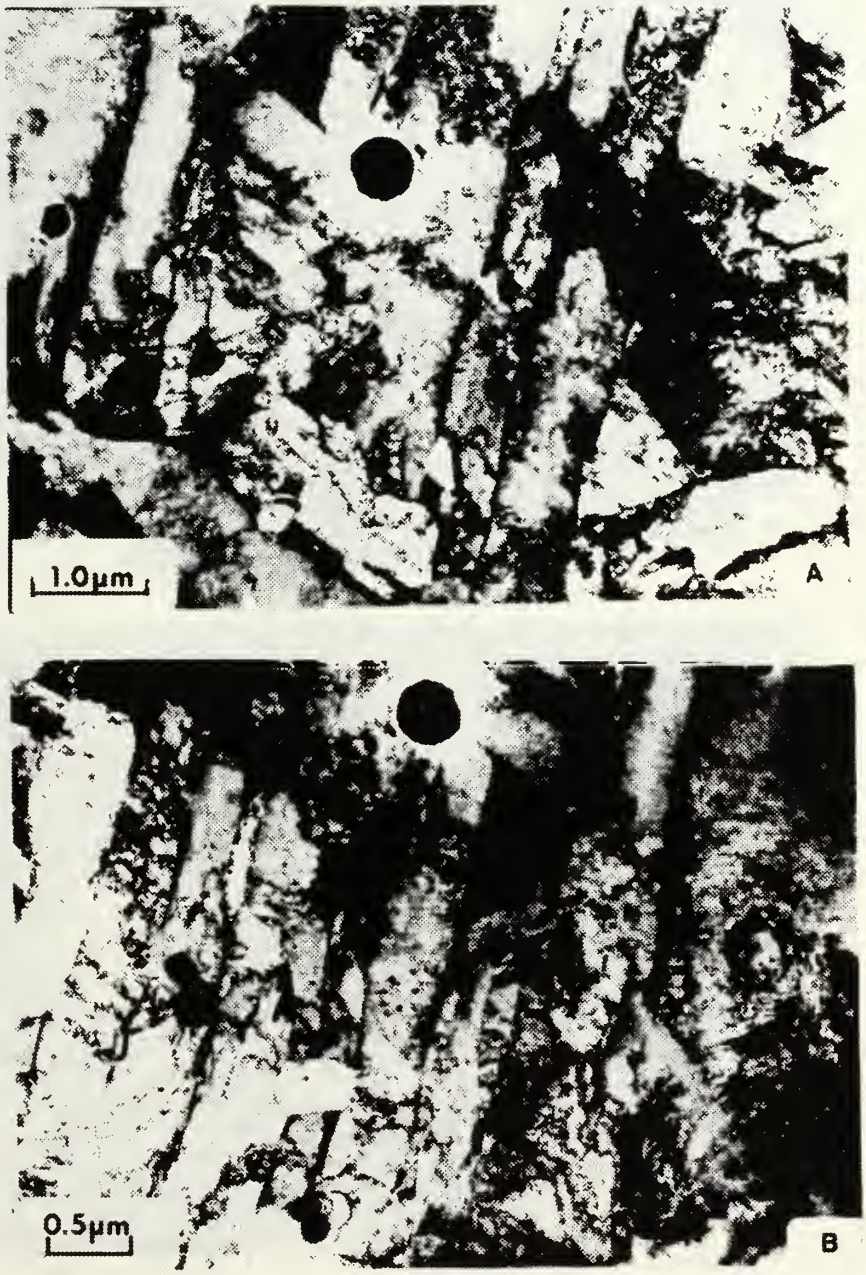

Figure 33. TEM Micrograph of W125
A.) Inclusion and Laths and Retained Austenite in the Weld Metal
B.) Inclusions, Lathes in Weld Metal

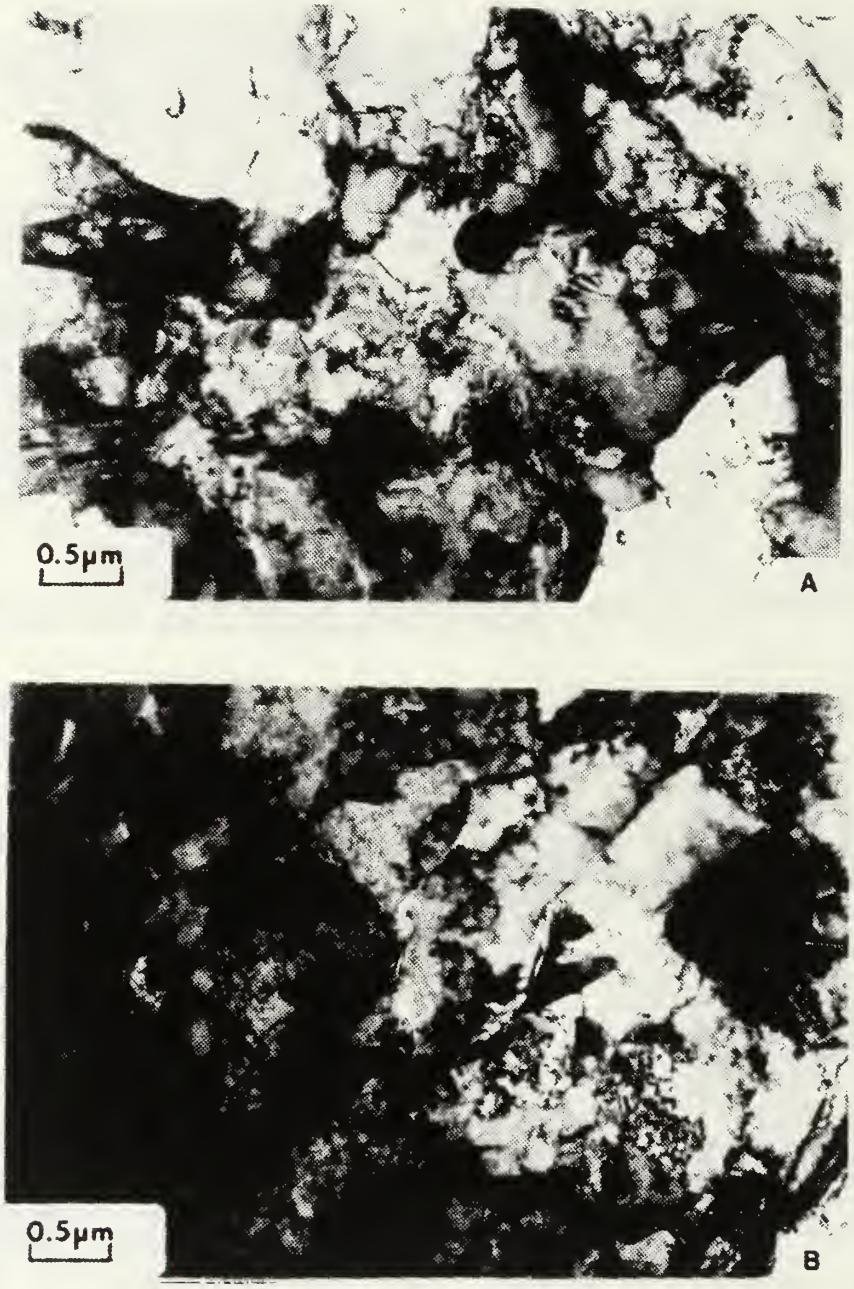

Figure 34. TEM Micrograph of
A.) Dislocations and Lathes in W119 Weld Metal Sample
B.) Inclusions and Large Grains on the W123 Fusion Line

Figure 35. TEM Micrograph of W119
A.) Dislocations and Laths in the Weld Metal
B.) Dislocations and Precipitates

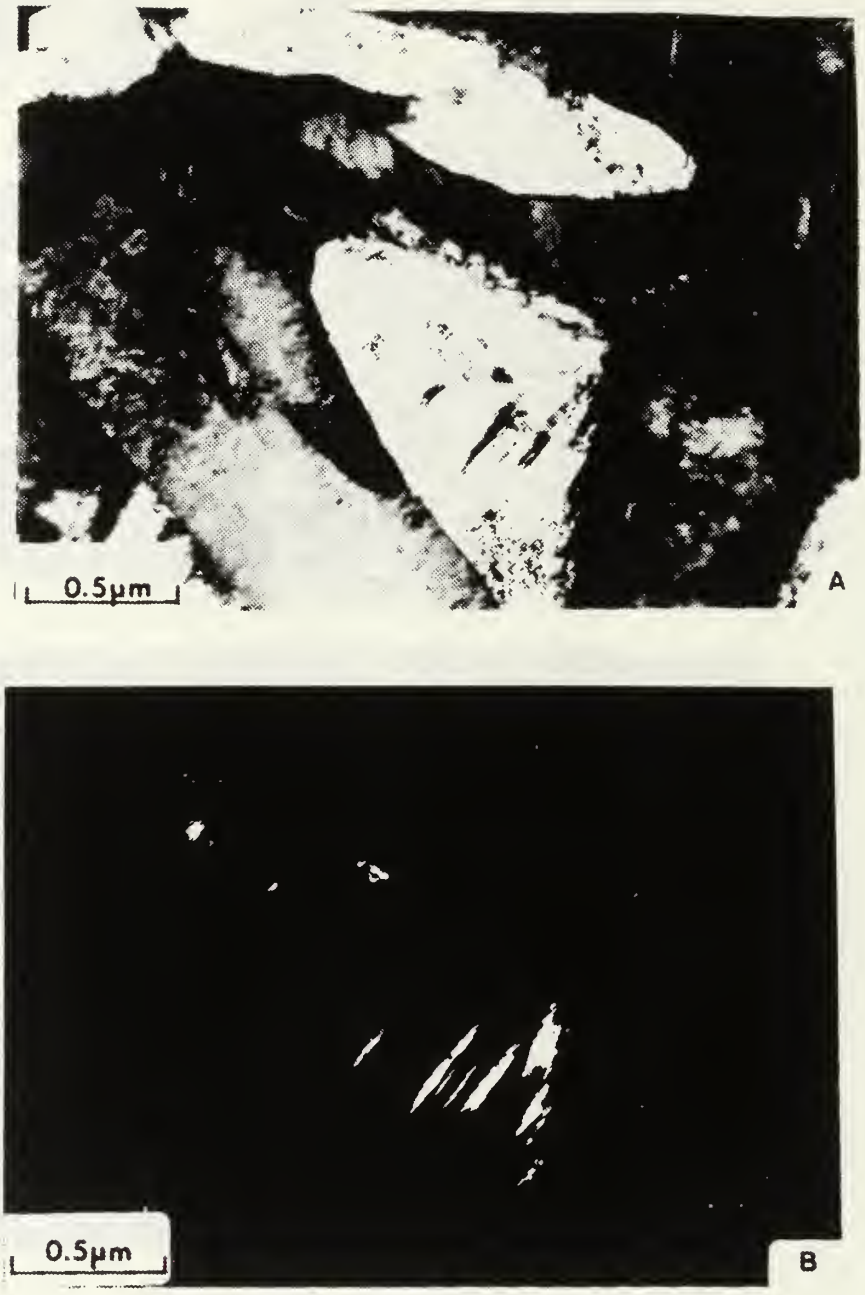

Figure 36. TEM Micrograph of W125
A.) Weld Metal
B.) Micro Twins

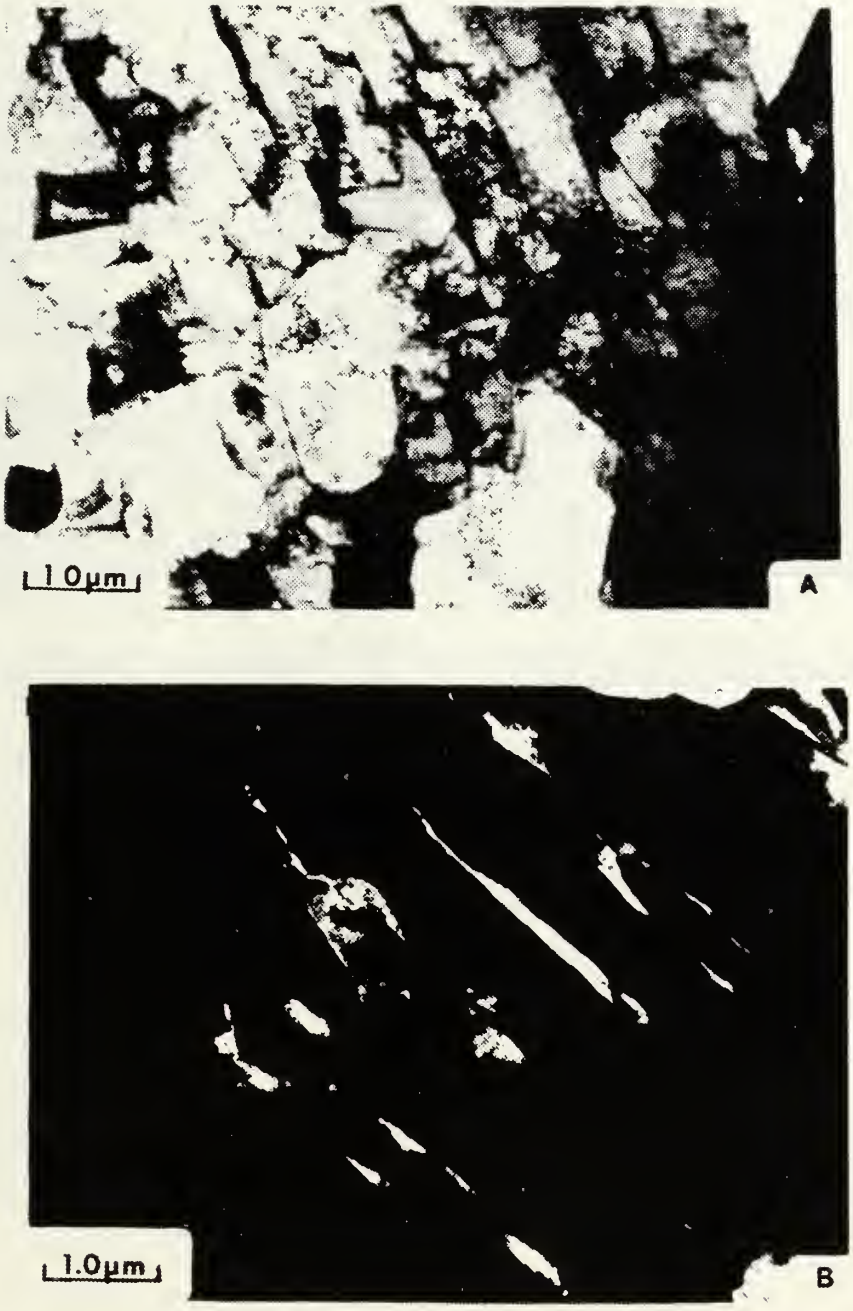

Figure 37. TEM Micrograph of
A.) W123 Weld Metal and Retained Austenite
B.) W119 Fusion Line TEM

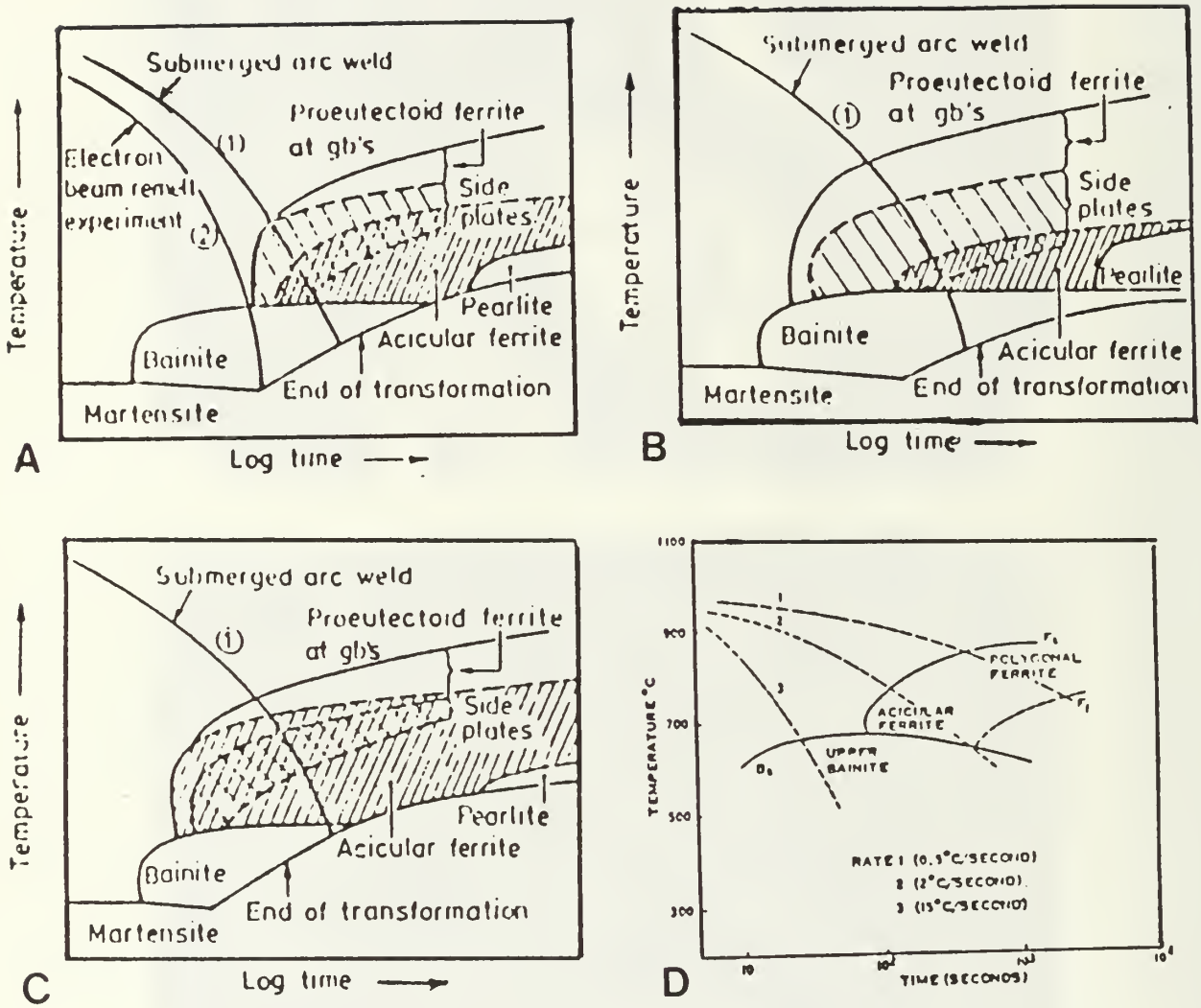

Figure 38. CCT curve for Oxygen Inclusions
A.) Low Oxygen Regime
B.) High Oxygen Regime
C.) Intermediate Oxygen Regime
D.) Schematic CCT Diagram

LIST OF REFERENCES

1. Anderson, T.L., Hyatt, J.A., West, J.C., "The Benefits of New High-Strength Low-Alloy (HSLA) Steels", Welding Journal, pp.21-26, September 1987.

2. Deb, P., Challenger, K. D., Burna , R. F., "Microstructural characterization of shielded metal arc weldments of a copper-bearing HSLA steel", Materials Science and Technology, pp. 1000-1006, November 1985.

3. Coldren, A.P., Cox, T.B. "Development of 100 KSI Yield Strength HSLA Steel", Amax Materials Research Center Report DTNSRDC/SME-CR-07-86, p.4, July 1986.

4. Miglin, M.T., Hirth, J.P., Rosenfield, A.R., Clark, W.A.T., "Microstructure of a Quenched and Tempered Cu-Bearing High-Strength Low-Alloy Steel", Metallurgical Transactions A, pp. 791-798, May 1986.

5. Glover, A. G., McGrath, J.T., Tinkler, M.J., Weatherly, G.C., "The Influence of Cooling Rate and Composition on Weld Metal Microstructures in a C/Mn and a HSLA Steel", Welding Journal, pp. 267-273 September 1977.

6. Easterling, K., Introduction to the Physical Metallurgy of Welding, p. 150, Butterworths & Co Ltd. London, 1983.

7. Wong, R.J., "Weld Process Development and Weldability of HSLA-100 Steel, Interim Report" DTNSRDC Report TM-28-87-09 , March 1987.

8. Abson, D.J., Dolby, R.E., "Microstructural Transformations in Steel Weld Metals - a Reappraisal", Welding Institute Research Bulletin, Volume 19 Number 7, p. 203, July 1978.

9. Ricks, R.A., Howell, P.R., Barritte, G.S., "The Nature of Acicular Ferrite in HSLA Steel Weld Metals", Journal of Materials Science 17 pp. 732-740, 1982.

10. Harrison, P.L., Farrar, R.A., "Influence of Oxygen -Rich Inclusions on the Austenite-Ferrite Phase Transformation in High-Strength Low-Alloy (HSLA) Steel Weld Metals". Journal of Materials Science 16, pp. 2218-2226, 1981.

INITIAL DISTRIBUTION LIST

1.	Defense Technical Information Center Cameron Station Alexandria, Virginia 22304-6145	2
2.	Library, Code 0142 Naval Postgraduate School Monterey, California 93943-5002	2
3.	Department Chairman, Code 69 Department of Mechanical Engineering Naval Postgraduate School Monterey, California 93943	1
4.	Associate Professor K.D. Challenger, Code 69Ch Department of Mechanical Engineering Naval Postgraduate School Monterey, California 93943	5
5.	Mr. Richard J. Wong, Code 2821 David Taylor Research and Development Center Annapolis, Maryland 21402	1
6.	K.D. Mickelberry Engineering Department USS Midway CV-41 FPO San Francisco, California 96601	3
7.	Mr. Paul Holsberg, Code 2821 David Taylor Research and Development Center Annapolis, Maryland 21402	1
8.	Lt. Gary P. Potkay, USN Class # 4-87B Engineering Duty Officer School Mare Island, Vallejo California 94592-5018	1
9.	Mr. John Pepe, Code 133.4 Welding Engineering Branch Long Beach Naval Shipyard Long Beach, California 90822	1

Th
18767 3

KNOX LIBRARY
NAVAL POSTGRADUATE SCHOOL
MONTEREY, CALIFORNIA 93943-5002

1 FEB 90

Thesis
M575355 Mickelberry
c.1 Microstructural
characterization of
HSLA-100 GMA-weldments.

7 NOV 88
3 OCT 89
1 FEB 90
6 FEB 91
4 FEB 93

33598
32719
35755
35572
37730

Thesis
M575355 Mickelberry
c.1 Microstructural
characterization of
HSLA-100 GMA-weldments.

thesM575355
Microstructural characterization of HSLA
3 2768 000 79189 1
DUDLEY KNOX LIBRARY